Solid-State Electronics Pergamon Press 1970. Vol. 13, pp. 759–788. Printed in Great Britain

THERMAL AND OPTICAL EMISSION AND CAPTURE RATES AND CROSS SECTIONS OF ELECTRONS AND HOLES AT IMPERFECTION CENTERS IN SEMICONDUCTORS FROM PHOTO AND DARK JUNCTION CURRENT AND CAPACITANCE EXPERIMENTS*

C. T. SAH, L. FORBES, L. L. ROSIER and A. F. TASCH, JR.

Department of Electrical Engineering and Materials Research Laboratory, University of Illinois, Urbana

(*Received* 7 *July* 1969; *in revised form* 17 *September* 1969)

Abstract—Photo and dark current and capacitance transient experiments are described which can provide highly accurate and unique data of the electronic properties of impurity centers in semiconductors such as energy level, multiplicity of charge state, thermal and optical emission rates, thermal capture rates, thermal and optical cross sections and the dependences of the rates and cross sections on sample temperature, static electric field and photon energy. These experiments are grouped into four categories in the discussion according to the temperature (below and above freeze-out or negligible and finite thermal rates) and presence or absence of optical excitation at the impurity center. Each category is subdivided into a number of cases according to the method used to set the initial charge state of the impurity center prior to the measurements. Methods of setting the initial state include electrical switching of the bias voltage and optical excitation using either interband or band to impurity monochromatic light. Experimental examples are given for many of the experiment methods discussed.

Résumé—On décrit des expériences avec des courants photoélectriques et de fuite ainsi que des capacités transitoires pour fournir des données très exactes des propriétés électroniques des centres d'impuretés des semiconducteurs. Ces propriétés comprennent: le niveau d'énergie, la multiplicité des états de charge, les taux d'émission optiques et thermiques, les surfaces transversales optiques et thermiques et les dépendances des surfaces transversales et taux d'emission en fonction de la température de l'échantillon, le champ électrique statique et l'énergie de photon. Ces expériences sont groupées dans la discussion en quatre catégorie d'après la température (au-dessous et au-dessus du dégel ou aux taux thermiques finis ou négligeables) et la présence ou absence d'excitation optique au centre d'impureté. Chaque catégorie est sous-divisée en un nombre de cas d'après la méthode employée pour fixer l'état de charge initial du centre d'impuretés avant les mesures. Les méthodes pour fixer l'état initial comprennent la commutation électrique de la tension de polarisation et l'excitation optique employant soit la lumière interbande ou la lumière à bande d'impureté monochrome. Des exemples expérimentaux sont donnés pour plusieurs des méthodes experimentales données.

Zusammenfassung—Photo- und Dunkelstrom sowie kapazitive Effekte werden beschrieben, die für Störstellen in Halbleitern sehr genaue Daten liefern über deren elektronische Eigenschaften wie Energieniveau, Multiplizität der Ladung, thermische und optische Emissionsraten, thermische Eingangsraten, thermische und optische Eingangsquerschnitte, sowie die Abhängigkeit der Übergangsraten und Wirkungsquerschnitte von Temperatur, statischen elektrischen Feldern und der Photonenenergie. Die Experimente werden in der Diskussion eingruppiert in vier Kategorien entsprechend einer Temperatur über oder unter dem Ausfrierpunkt bzw. vernachlässigbarer oder endlicher thermischer Raten und entsprechend der Existenz oder Nichtexistenz einer optischen Anregung beim Störzentrum. Jede Kategorie ist unterteilt in eine Anzahl von Fällen je nach der

* Supported in part by the Advanced Research Projects Agency and the Air Force Office of Scientific Research.

verwendeten Methode zur Festlegung des Ausgangszustandes der Ladung der Störstellen vor der Messung. Unter diesen Methoden sind aufgeführt, das An- und Abschalten einer elektrischen Vorspannung an der Probe und eine monochromatische optische Anregung durch Band- Band- und Band-Term-Übergänge. Für viele der diskutierten Bestimmungsmethoden werend experimentelle Beispiele angegeben.

NOTATION

A	junction area
c_n, c_p	total capture rate of electrons or holes, $c_n = c_n^0 + c_p^t$
c_n^0, c_p^0	radiative capture rate of electrons or holes
c_n^t, c_p^t	thermal capture rate of electrons or holes
$C(t)$, C	time dependent and steady state high frequency junction capacitance
e_n, e_p, e_n^0, e_p^0, e_n^t, e_p^t	emission rates corresponding to the c's defined above
E	defined after (6.12)
E_C, E_V, E_T, E_D, E_A, E_I	energy levels of conduction band edge, valence band edge, imperfection or trap center, donor center, acceptor center and the intrinsic Fermi level
F_N, F_P	steady state quasi Fermi levels of electrons and holes
G_I	steady state interband electron–hole optical generation rate
$\hbar$	Planck's constant
I, $i(t)$	steady state and time dependent junction current
i_{cn}, i_{cp}	the conductive parts of the junction current due to electron and hole transit
i_d	the displacement part of the junction current
i_r, i_c, i_h, i_R, i_F	defined in Fig. 6
i_{ON}, i_{OFF}	defined in (6.6), junction current when the light is turned on or off
I_R	steady state junction reverse current
I_J, i_j, i_J	steady state, time dependent and total junction current
J_N, J_P, J_R	electron, hole and total reverse steady state junction current density
k_B	Boltzmann factor
N, P, N_E, P_E, n, p	steady state, equilibrium and total electron and hole concentration
N_T, P_T, n_T, p_T	steady state and total trapped electron and hole concentrations
N_0, P_0	initial electron and hole concentrations
n_1, n^*, p^*	electron or hole concentration when $E_F = E_T$ or $E_F = E_T^*$
n_i	intrinsic carrier concentration
nA	nanoampere
N_I, N_D, N_A, N_{TT}	ionized impurity, donor, acceptor and deep level imperfection center concentrations
q	electronic charge
s	number of electrons trapped at an impurity center referred to its neutral state
S, S_{ON}, S_{OFF}	the step rise or fall ($S = S_{ON}/S_{OFF}$) during the turn-on or turn-off phase in the high temperature photocurrent experiment
t	time
t_R, t_S, t_1	defined in Fig. 6
t_{tr}, t_d	transit time and dielectric relaxation time
T, T_J, T_F	junction temperatures
x	space coordinate in the junction
V	applied junction voltage
V_J, v_J, v_J	applied junction voltage, steady state, time dependent, total
V_R	steady state reverse junction voltage
V_D	diffusion or contact potential of the junction
v_n, v_s	thermal velocity of electron and saturation velocity in high field
W, $w(t)$	width of the junction transition region
W_0, W_∞	initial and final width of the junction transition region
$K_S\epsilon_0$	dielectric constant of semiconductor
α_n^0, α_I	optical absorption coefficient of trapped electron and valence electron
σ_n^0 σ_n^t,	optical and thermal cross sections of electron
σ_{p0}^t σ_{n0}^t σ_{p1}^t	thermal capture cross sections of electrons and holes at $s = 0$ and $s = 1$ charge states
τ, τ_{ON}, τ_{OFF}	turn-on and turn-off exponential decay time constants
μ_n	electron mobility
λ	wavelength of light

1. INTRODUCTION

THE ELECTRICAL and optical properties of imperfections such as impurity centers in semiconductors are characterized by the energy level scheme and the electronic transition probabilities between the defect states and the conduction and valence band states. While the energy levels of the ground and excited states of shallow level centers have been measured with considerable precision in Si and Ge from infrared absorption studies,[1] those of the deep level impurity centers determined from the thermal activation energy of Hall constant and conductivity measurements are uncertain by several tens of millivolts. Similarly, optical absorption cross sections for shallow levels have been measured

quite extensively but rarely for deep level impurities. Most of the data for deep level centers in Si and Ge are usually given as relative photoresponse.[2]

The experimental status of the thermal cross sections of electrons and holes at impurity centers is the least satisfactory among these parameters. Published data vary over several orders of magnitude from different experiments and laboratories,[3] supposedly for identical impurity species and electric field or sample temperature. The difficulties lie in both the accuracy of determining the impurity concentration and in the nonlinear model used for the analysis of the kinetic decay data.

It has been shown that the impurity photovoltaic effect in the depletion region of a semiconductor junction can provide a unique and precise determination of these thermal and optical cross sections without the uncertainties associated with the older method.[4] In this paper, a detailed theory of this method will be given. In addition, extension of this method to include dark current transient with or without carrier freeze-out at low temperature and dark and photocapacitance transients will also be discussed. It will be shown that these methods, all applied to a given semiconductor junction sample, can provide detailed information of the impurity center with high precision. Properties such as the thermal and optical cross sections, energy levels including the multiplicity of charge states, electric field and temperature dependences of the emission rates and cross sections, and spatial dependence of the impurity or defect concentration can be obtained.

The theory of each of these methods will be presented and followed by an experimental example or discussion of experimental result when available. Predicted dark and photo capacitance and current transient waveforms will be given for a single level acceptor or donor center in each method.

2. CLASSIFICATIONS OF EXPERIMENTS

Because of the large number of possible experiments, it is desirable to give a summary of the various types of experiments which can yield useful information on the thermal and optical properties of the defect center. To facilitate this discussion, the energy level diagram of a defect center is shown in Fig. 1. The semiconductor

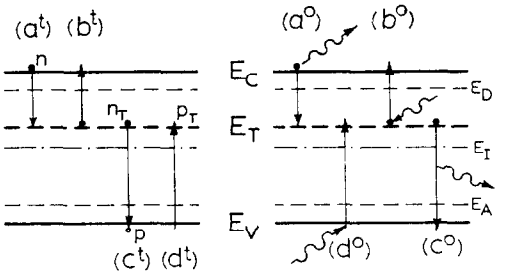

FIG. 1. The energy band diagram and the four thermal and four optical transition processes between the impurity and a band state.

conduction and valence band edges are denoted by E_C and E_V while the shallow level impurities have energy levels E_D and E_A for the donors and acceptors respectively. Their concentrations are N_D and N_A and it is assumed that they are completely ionized. When deionization occurs at low temperatures, N_D and N_A should be replaced by N_{D+} and N_{A-}, the ionized impurity concentrations. The deep level imperfection center to be analyzed in detail here has an effective energy level denoted by E_T which includes both the excited states and their degeneracies. The excited states are not populated since their energy separation from the ground state is considerably greater than k_BT when experiments are performed below about 100°C. The degeneracy factor of the ground state is included in E_T for the thermal processes and its value depends on a particular approximation of counting of states for a given atomic model. This question will be discussed in a subsequent paper where extensive experimental data are obtained for a given impurity center, such as gold in silicon.[5] The concentrations of the electrons in the conduction band is denoted by $n(x, t)$ and holes by $p(x, t)$ while those trapped at the impurity center, E_T, are denoted by $n_T(x, t)$ and $p_T(x, t)$. The center is assumed to have only two charged states. For acceptor-like centers, these are $s = 1$ (the acceptor charge state with one negative electronic charge) and $s = 0$ (the neutral charge state). For donor-like centers, the charge states are $s = 0$ (the neutral charge state) and $s = 1$ (the donor charge state with one positive electronic charge. s denotes the number of electrons trapped at the impurity or defect center.

The transition processes and their transition rates are also indicated in Fig. 1 where (a^t), (b^t), (c^t) and d^t) are the four thermal processes while (b^0) and (d^0) are the two optical excitation processes. The radiative recombination processes, (a^0) and (c^0), have negligible rates in indirect materials such as Si and Ge but are important in direct materials such as GaAs, especially when carrier concentration is high. In these experiments, the carrier concentrations are negligible during the transient phase so that the radiative captures can be neglected. Note that the arrows indicate direction of electronic transition. Sometimes, it is convenient to indicate the direction of hole transition for those involving the valence band.

The transition rates are denoted by c and e respectively with appropriate subscript, n or p for electrons or holes, and superscript, t or 0 for thermal or optical processes. Thus, ${c_n}^t$ and ${e_n}^t$ are the thermal capture and emission rates of electrons at an unfilled and filled center respectively while ${c_n}^0$ and ${e_n}^0$ are the radiative capture and photo-emission (or photo-excitation) rates of electrons. For the types of kinetic measurements to be discussed, these coefficients are sufficient to completely describe the rate equations of the eight electron and hole emission and capture processes at the defect center as indicated in Fig. 1. The detailed dependence of these rate constants on the band model and on the photon wave length for the optical rate constants will not be discussed here, however, a detailed discussion of the atomic model will be made in subsequent papers where detailed data are presented for temperature and electric field dependences for gold[5], sulfur[6] and other imperfections.

The rate equations which describe these eight processes are essential in the detailed analysis of the experimental data. These are given below.

$$-(\mathrm{d}n/\mathrm{d}t)_T = (a^t)-(b^t)+(a^0)-(b^0)$$
$$= {c_n}^t n p_T - {e_n}^t n_T + {c_n}^0 n p_T - {e_n}^0 n_T$$
$$\equiv c_n n p_T - e_n n_T \qquad (2.1\mathrm{A})$$

$$-(\mathrm{d}p/\mathrm{d}t)_T = {c_p}^t p n_T - {e_p}^t p_T + {c_p}^0 p n_T - {e_p}^0 p_T$$
$$\equiv c_p p n_T - e_p p_T \qquad (2.1\mathrm{B})$$

$$(\mathrm{d}n_T/\mathrm{d}t) = (a^t)-(b^t)+(a^0)-(b^0)-(c^t)+(d^t)$$
$$-(c^0)+(d^0)$$
$$= (c_n n + e_p)p_T - (c_p p + e_n)n_T$$
$$= -(c_n n + e_n + c_p p + e_p)n_T$$
$$+(c_n n + e_p)N_{TT}. \qquad (2.1\mathrm{C})$$

Here, $(\mathrm{d}n/\mathrm{d}t)_T$ and $(\mathrm{d}p/\mathrm{d}t)_T$ given by (2.1A) and (2.1B) denote the rate of change of carrier concentrations in the bands due to these thermal and optical processes at the defect centers and they do not include those due to other generation–recombination processes and to currents. The combined thermal and optical rate constants are denoted by c_n, c_p, e_n and e_p where $c_n = {c_n}^t + {c_n}^0$, etc. In obtaining the final form of (2.1C), use is made of the totality condition given by $N_{TT}(x) = n_T(x, t) + p_T(x, t)$.

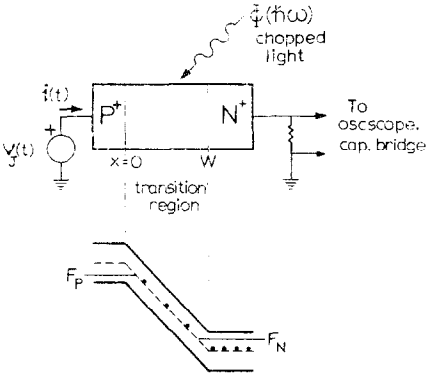

FIG. 2. Schematic diagram of the photoexperimental setup.

The experimental setup is shown in the schematic diagram in Fig. 2. The transition region of the p–n junction lies in $0 < x < w(t)$. Junction structures of the $P+N$, $N+P$ and $P+IN+$ types are used in actual experiments and each has some unique advantages in determining the various thermal and optical parameters of the defect centers. For the $P+IN+$ structure, the band diagram is shown in Fig. 2 with a constant field. Outside of the transition region, the field is assumed zero and electrical neutrality prevails. These approximations allow the use of the constant quasi-Fermi levels outside of the transition region. Inside the transition region, the constant quasi-

Fermi level approximation for electrons and holes is not valid when the junction is under large reverse bias.[7] The constant quasi-Fermi level approximation is adequate, however, since all that is necessary is the depletion condition $p = n = 0$ in the transition region during the transient experiments at large reverse junction bias voltages. For low temperature experiments when $e_n{}^t$ and $e_p{}^t$ are negligible, the solutions of (2.1A) to (2.1C) can also be simplified even if $n, p \neq 0$ in the transition region if they are stationary. This corresponds to carrier injection into the transition region either by light or by an adjacent and forward biased junction (transistor structure).[6]

The independent experimental parameters are: (1) junction voltage, $v_J(t) = V_J + v_j(t)$, (2) junction or sample temperature, $T_J(t)$, (3) photon flux, $\Phi(\hbar\omega, t)$. The quantities to be measured are: (1) Short circuit junction current, $i_J(t) = I_J + i_j(t)$ and (2) high frequency small signal junction capacitance, $C(t)$. Evidently, one could also measure the small signal junction conductance and the frequency dependences of both the small signal junction capacitance and conductance. However, the interpretation of these frequency dependences and their relationships to the thermal and optical emission rates and cross sections are complicated[8] and do not possess the simplicity which $i_J(t)$ and $C(t)$ have.

From Fig. 3, it is evident that a large number of temporal sequences of the three independent variables (voltage, temperature and monochromatic or multichromatic photon flux) can be arranged.

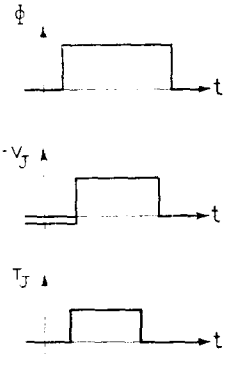

FIG. 3. A possible temporal sequence of the three independent variables, the photon flux ϕ, the junction voltage v_J and temperature T_J.

Each of these sequences will give a predictable junction current and capacitance transients which can then be used to obtain the thermal and optical parameters of the centers. Some of the relatively simple and important experimental conditions and the obtainable parameters are summarized in Table 1.

For example, experiments 1*c* and 1*i* (c = capacitance, i = current) are performed at a temperature below the freeze-out temperature, T_F, of the defect centers so that the thermal emission rates, $e_n{}^t$ and $e_p{}^t$, are very small and negligible. The trapped charge concentration, n_T, can then be assumed stationary. In these experiments, the junction voltage is switched from zero to a large reverse bias value, $-V_R$, as indicated in the column of $v_J(t)$ in Table 1. The zero bias condition sets the *initial condition* of the trapped charge, $n_T(0)$, which is also stationary in this case. The experiments are then performed in the dark, $\Phi = 0$, and thermal radiation from the surroundings must be avoided. The data of I–V and C–V then allow the determination of N_D(or N_A) and N_{TT} as a function of position if data are obtained on both a control sample ($N_{TT} = 0$) and a sample doped with some N_{TT}.

The initial condition of $n_T(0)$ can be set by various means. The dark low temperature experiments listed under 2*c* and 2*i* in Table 1, set the initial condition of $n_T(0)$ by forward bias injection of minority carriers across the junction. This experiment provides a possibility of measuring the spatial variation of $n_T(x)$, $N(x)$ and $P(x)$. It will also give the ratio $c_n{}^t/c_p{}^t$ if the forward injection level is very high.

A second means of setting the initial condition of n_T is by optical generation. The low temperature experiments are listed under 3*c* and 3*i* in Table 1.

In the following sections, the details of each of the experiments listed in Table 1 are described and some examples of experimental results are given.

3. LOW TEMPERATURE DARK C–V and I–V EXPERIMENTS

In this section, we shall discuss the low temperature experiments in the dark which are listed under items 1, 2 and 3 in Table 1. Experiments 1*c* and 1*i* are those performed without carrier injection while experiments 2 and 3 are measurements performed after carrier injection either by forward biasing the

Table 1

Exp No.	$\Phi(\hbar\omega, t)$	$v_J(t)$	T_J	Data	$e_n{}^t$	$e_p{}^t$	ΔE_T	$e_n{}^0$	$e_p{}^0$	$c_n{}^t$	$c_p{}^t$	N_I	N_D	N_{TT}	Fig.
1*c*	0	$-V_R 0 - V_R$	$< T_F$	*C–V*	*R*	*R*	—	—	—	—	—	*X*	*X*	*X*	4
1*i*	0	$-V_R 0 - V_R$	$< T_F$												4
2*c*	0	$+V_F 0 - V_R$	$< T_F$	*C–V*	*R*	*R*				*R*	*R*				6
2*i*	0	$+V_F 0 - V_R$	$< T_F$												6
3*c*-1	$\hbar\omega > E_G$	$-V_R 0 - V_R$	$< T_F$	*C–V*	*R*	*R*				*R*	*R*				7
3*c*-2	$\hbar\omega \gg E_G$	$0 - V_R$	$< T_F$	*C*(*t*)						*X*	*X*	*X*	*X*	*X*	8
4*c*	0	$0 - V_R 0$	$> T_F$	*C*(*t*)	*R*	*R*	*X*					*X*	*X*	*X*	10
4*i*	0	$0 - V_R 0$	$> T_F$	*i*(*t*)	*X*	*X*	*X*			*X*	*X*				10
5*c*	0	$+V_F - V_R$	$> T_F$	*C*(*t*)	*R*	*R*	*X*			*R*	*R*	*X*	*X*	*X*	13
5*i*	0	$+V_F - V_R$	$> T_F$	*i*(*t*)	*X*	*X*	*X*			*X*	*X*				13
6*c*	$\hbar\omega > E_G$	$0 - V_R$	$> T_F$	*C*(*t*)	*R*	*R*	*X*			*R*	*R*				
6*i*	$\hbar\omega > E_G$	$0 - V_R$	$> T_F$	*i*(*t*)	*X*	*X*	*X*			*X*	*X*				
7*c*	$\hbar\omega > \Delta E_T$	$0 - V_R$	$< T_F$	*C*(*t*)			*X*	*R*	*R*			*X*	*X*	*X*	15
7*i*	$\hbar\omega > \Delta E_T$	$0 - V_R$	$< T_F$	*i*(*t*)			*X*	*X*	*X*	*X*	*X*				15
8*c*	$\hbar\omega > \Delta E_T$	$+V_F 0 - V_R$	$< T_F$	*C*(*t*)			*X*	*R*	*R*	*R*	*R*	*X*	*X*	*X*	17
8*i*	$\hbar\omega > \Delta E_T$	$+V_F 0 - V_R$	$< T_F$	*i*(*t*)			*X*	*X*	*X*	*X*	*X*				17
9*c*	$\hbar\omega_1 > E_G$	$0 - V_R 0$	$< T_F$	*C*(*t*)			*X*	*R*	*R*	*R*	*R*	*X*	*X*	*X*	18
9*i*	$\hbar\omega_2 > \Delta E_T$			*i*(*t*)			*X*	*X*	*X*	*X*	*X*				18
10*c*	$\hbar\omega > \Delta E_T$	$0 - V_R$	$> T_F$	*C*(*t*)	*R*	*R*	*X*	*R*	*R*						19
10*i*	$\hbar\omega > \Delta E_T$	$0 - V_R$	$> T_F$	*i*(*t*)	*R*	*R*	*X*	*R*	*R*						19
10*c*1	$\hbar\omega > \Delta E_T$	$0 - V_R$	$> T_F$	*C*(*t*)	*R*	*R*	*X*	*R*	*R*						22
10*i*1	$\hbar\omega > \Delta E_T$	$0 - V_R$	$> T_F$	*i*(*t*)	*X*	*X*	*X*	*X*	*X*						22
11*c*	$\hbar\omega > \Delta E_T$	$+V_F - V_R$	$> T_F$	*C*(*t*)	*R*	*R*	*X*	*R*	*R*	*R*	*R*				
11*i*	$\hbar\omega > \Delta E_T$	$+V_F - V_R$	$> T_F$	*i*(*t*)	*X*	*X*	*X*	*X*	*X*	*X*	*X*				
12*c*	$\hbar\omega > E_G$	$0 - V_R$	$> T_F$	*C*(*t*)	*R*	*R*	*X*	*R*	*R*	*R*	*R*				
12*i*	$\hbar\omega > \Delta E_T$			*i*(*t*)	*X*	*X*	*X*	*X*	*X*	*X*	*X*				

R = ratio; X = value.

junction as in 2*c* and 2*i* or by interband optical excitation as in 3*c* and 3*i*.

3.1 *Experiment* 1, *no carrier injection*

The temporal sequences of junction temperature and voltage are illustrated in Fig. 4(b) and (c). The staircase junction voltage change represents the measurements of the *C–V* curve. The temperature drop from 300°K to a value below the freeze-out temperature at $t = 0$ is assumed to be rather rapid. The impurity centers in the transition region, $0 < x < W$ at $V = -V_R$ will all be in the steady state charge condition of 300°K and thus n_T $(0 < x < W) = N_{TT} e_p{}^t/(e_n{}^t + e_p{}^t)$, as shown in Fig. 4(g). The slight drop of C^2 at $t = 0$ comes from the increase of the barrier height due to the temperature dependence of V_D. For ideal P^+N or N^+P step junction with constant impurity concentration, this slight change is evident in

$$C^2 = qK_s\epsilon_0 A^2 N_I/2(V_D + V_R) \qquad (3.1)$$

where N_I is the ionized impurity concentration in the transition region whose width is given by*

$$W = \sqrt{[2K_s\epsilon_0(V_D + V_R)/qN_I]} \qquad (3.2)$$

$K_s\epsilon_0$ is the dielectric constant of the semiconductor and A is the junction area.

At t_1, the junction voltage is switched back to zero as indicated in Fig. 4(b) so that $n_T(W_0 < x < W) \doteq N_{TT}$. When it is rapidly switched from 0 to $-V_R$ at t_2 the impurity centers in this transition region will remain filled as illustrated in Fig. 4(i). Thus, $N_I = N_D - N_{TT}$ for

* A more accurate solution for the $P+N$ junction with high concentration of N_{TT} is given in Appendix A.

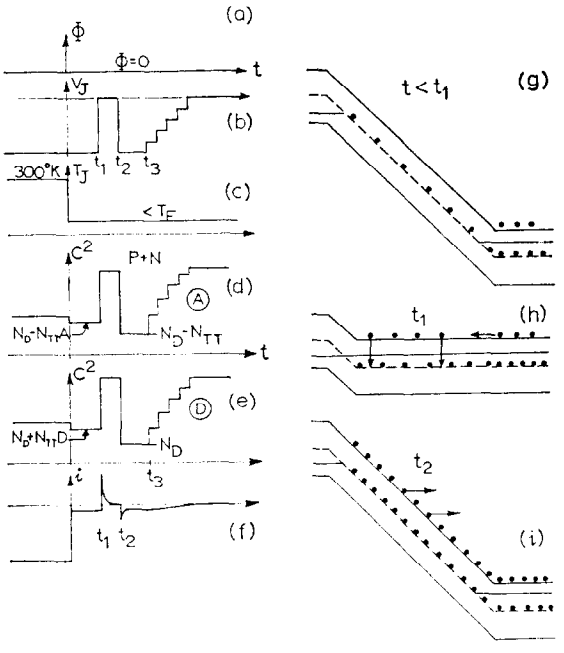

FIG. 4. The low temperature dark C–V and I–V experiments, (a), (b) v_J, (c) T_J, (d) C^2 for single level acceptor center in P^+N junction, (e) C^2 for single level donor center in P^+N junction, (f) $i(t)$, (g) steady state energy band for large reverse bias, (h) for zero bias and (i) for large reverse bias just after switching from zero bias at t_2, indicating majority carrier (electron) swept-out by the high field. $A = e_p{}^t/(e_p{}^t+e_n{}^t)$ $D = e_n{}^t/(e_p{}^t+e_n{}^t)$.

acceptor impurity centers while $N_I = N_D$ for donor impurity centers in a P^+N diode. Expressions of N_I are listed in Table 2 for the four cases of single-level impurity centers. It is evident from this discussion and from Fig. 4(d) and (e) that the difference of capacitance before and after switching to $V = 0$ will provide numerical result for $N_{TT}e_n{}^t/(e_n{}^t+e_p{}^t)$ at 300°K.

Table 2. The initial value of the ionized impurity concentration in the transition region for donor-like and acceptor-like defect centers in P^+N and N^+P diodes

$N_I(0+)$	P^+N	N^+P
Donor	N_D	N_A-N_{TT}
Acceptor	N_D-N_{TT}	N_A

During the voltage switching from $-V_R$ to 0 to $-V_R$ at t_1 and t_2, there are fast current transients corresponding to majority carriers moving into the transition region as illustrated in Fig. 4(h) and (i). In these energy band diagrams, constant field is assumed for simplicity of illustration although for the P^+N and N^+P step junction case with N_A and N_D spatially constant, the field is linearly varying with distance. The switch-off transient ceases in about a dielectric relaxation time of the majority carriers while the switch-on transient at t_2 elapses in about a carrier transit time across W with saturated velocity. These are of the order of 10^{-10} sec and can be disregarded in the capacitance measurements.

In $t > t_3$, the high frequency C–V data is obtained. The slope of the C^{-2} vs. V_R curve then gives the total ionized impurity concentration as indicated in (3.1). The value of N_I can also be obtained from the value of C directly if V_D is known or if V_R is large compared with V_D, which is usually of the order of 1 V.

From the C–V data on a control sample, the value of N_D or N_A can be determined. This can then be used with the C–V data of a sample doped with the impurity centers to give N_{TT}. In addition, if the center is a simple one-level impurity, Table 2 shows that the C–V data can also be used to determine the charge state (acceptor-like or donor-like) of the impurity center. For example, in gold-doped Si diodes, there are three gold charge states,[9] an acceptor, a neutral and a donor state. Thus, the P^+N diode can be used to determine the gold concentration via the acceptor center while the N^+P diode can be used to determine the gold concentration via the donor center.

The method just described assumes that $N_{TT} \ll N_D$ or N_A and that both N_{TT} and N_D or N_A are spatially constant. The method can be extended to evaluate the spatial dependence of N_{TT} and N_D or N_A by the well-known technique of using the slope dC/dV. For a given reverse bias, V_R, the position W of $N_I(W)$ can be determined from the capacitance measurement using

$$W = K_s\epsilon_0 A/C \tag{3.3}$$

and the total ionized impurity concentration at W is given by

$$N_I(W) = -(C^3/qK_s\epsilon_0 A^2)/(dC/dV) \tag{3.4}$$

Analysis of the data of both a control sample and a gold doped sample will then give both $N_D(x)$ and $N_{TT}(x)$.

Experimental data of gold doped Si P^+N step junction are given in Fig. 5(a). Gold was diffused into the sample at 840°C for 48 hr and the junction area is 4.5×10^{-3} cm^2 (a 30 mil dia. dot). The figure shows the measurements for both a control sample and a gold doped sample at both 23°C and 77°K. The slight nonlinearity of the data comes from the diffused boron profile of the P^+ region.

Curves (A) and (B) are for the gold doped diode while curve (C) is the control diode. Curve (A) corresponds to the experimental condition after t_0 indicated in Fig. 4: the diode is at $T = 77$°K and $V = 0$ V and a reverse bias of $V = -V_R = -60$ V is then applied to the sample. Thus, all of gold atoms in the transition region $W_0 < x < W$ are frozen into the acceptor charge state giving $N_I = N_D - N_{TT}$ as illustrated in Fig. 4(ii). The slope of curve (A), using (3.1), then gives $N_I = N_D - N_{TT} = 6.24\times10^{14}$/cm^3.

Curve (B) corresponds to two sets of experimental data: (1) 23°C data of gold doped sample and (2) condition shown in Fig. 4 from $t < 0$ to $0 < t < t_1$, and C–V data afterwards. The fact that these two experimental conditions give the same results at large V_R indicates that the gold charge state in $0 < x < W$ must be the same at these two temperatures. Thus, from $N_I = N_D - N_{TT}e_p{}^t/(e_p{}^t + e_n{}^t)$, we conclude that either $e_p{}^t/e_n{}^t \ll 1$ or $e_p{}^t/e_n{}^t$ is independent of temperature from 23°C to 77°K. The former is the case for the gold acceptor center as suggested by the fact that the control sample given by curve (C) is nearly identical to the gold doped sample of curve (B). This is consistent also with measurements described in subsequent sections and with published data.[10] The temperature dependence of $e_p{}^t/e_n{}^t$ cannot be determined from the present experiments.

From curve (B) and using (3.1), we have $N_I = N_D - N_{TT}e_p{}^t/(e_p{}^t + e_n{}^t) = 9.12\times10^{14}$/cm^3. Combine this with the result of curve (A) taken on the same diode, we have $N_{TT}e_n{}^t/(e_n{}^t + e_p{}^t) = 2.88\times10^{14}$/cm^3 which is consistent with the solid solubility data at the gold diffusion temperature,[11] which is 1.5×10^{15}/cm^3.

For the control sample given by curve (C) in Fig. 5(b), the donor impurity concentration is $N_D = 8.48\times10^{14}$/cm^3, which is too low compared with what would be expected from the result of curve (B) given above. This error arises due to the variation of N_D among various diode samples from the radial distribution of N_D during crystal growth. To obtain more accurate results, it is necessary to use adjacent diodes for the control and the gold doped samples.

In view of the slight nonlinearity of the C^{-2} vs. V_R curves, the positional dependences of N_I of curves (A) and (B) of Fig. 5(a) are evaluated using

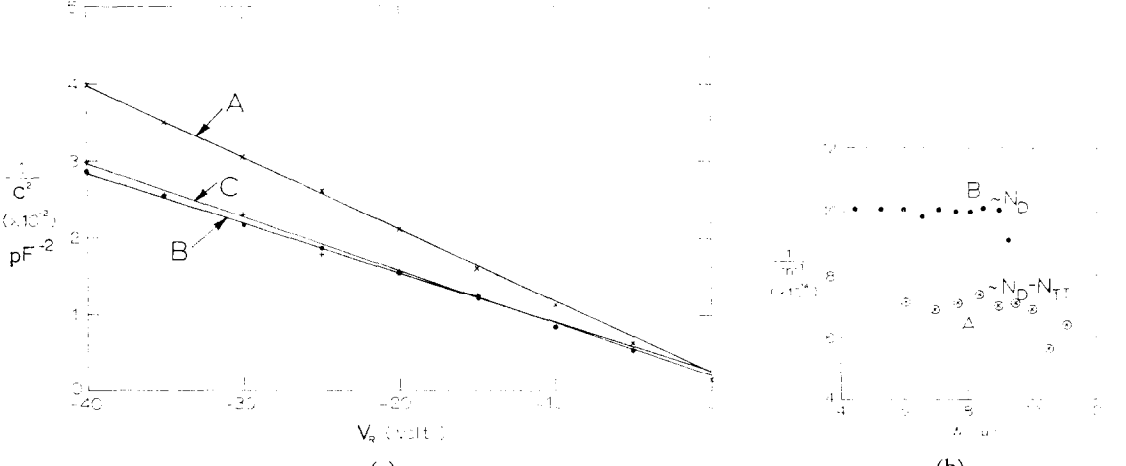

(a) (b)

FIG. 5. Experimental data of P^+N diodes in Si. (a) curves A, B and C see text, (b) N_D and $N_D - N_{TT}$ vs. W by varying V_R.

(3.3) and (3.4). These are shown in Fig. 5(b) and their differences, giving $N_{TT}e_n{}^t/(e_n{}^t+e_p{}^t)$, are also shown. The difference curves indicate that N_{TT} is quite constant over the entire transition region of about 10 μm wide.

3.2 *Experiments* 2, *carrier injection by forward bias*

The initial condition of the trapped charge concentration in the transition region of the p–n junction can be altered either electrically or optically by injecting or generating a high concentration of electrons and holes. Under this condition, the trapped electron concentration will depend on the ratio of the capture rates $c_n{}^t/c_p{}^t$ so that information on the capture rate can be obtained. Injection by forward biasing the junction would give a spatial dependence of the injected carrier concentration which can be measured from the C–V and dC/dV data using (3.4A) and (3.4B).

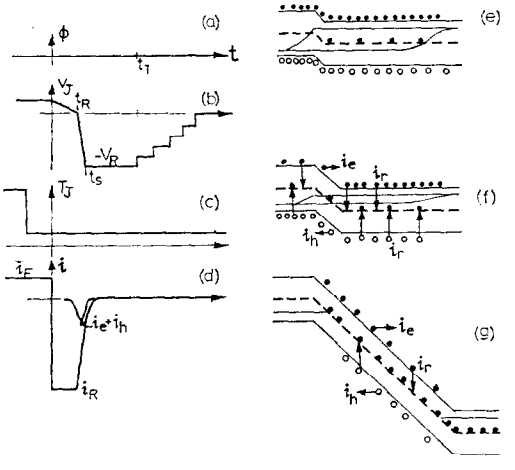

FIG. 6. The low temperature dark experiments with forward bias injection. (a) light flux, (b) junction bias voltage, (c) temperature, (d) current, (e) charge distribution during forward bias, (f) charge at $0 < t < t_R$ and (g) charge and current at $t_R < t < t_S$

The experimental conditions are described in Fig. 6(a–f). At $t = 0$, the applied voltage (through a series resistance) is switched from $+V_F$ to $-V_R$. The junction voltage will however experience a delay due to the presence of the injected carriers which must recombine. These are illustrated by i_R in Fig. 6(f) and the current is limited by the external circuit: $i_R = V_R/R_L$ where R_L is the load resistance. This part of the current is well-known in the theory and application of the pulse recovery diode current method for the determination of the recombination lifetime since the length of the reverse phase, t_R shown in Fig. 6(d), is proportional to the minority carrier lifetime.[12] There are two additional fast components due to carrier sweep-out. These are illustrated in Fig. 6(f) and (g) by i_e i_h and sketched in Fig. 6(d). They are similar to those shown in Fig. 4(f) and are swept-out in the order of the transit time across W.

At the end of these fast transients, the carrier concentrations in the middle part of the transition region may still be considerably higher than the doping N_D or their equilibrium values, N_E and P_E. Thus, the trapped charge concentration must be described by the general steady state value

$$N_T = N_T(x) = \frac{N_{TT}(c_n{}^t N + e_p{}^t)}{c_n{}^t N + e_n{}^t + c_p{}^t P + e_p{}^t} \qquad t \geq t_s \tag{3.5}$$

where $P = P(x)$ and $N = N(x)$. The C–V and dC/dV measurements can then be used to determine $N_T(x)$.

3.3 *Experiments* 3, *carrier generation by interband light*

Instead of carrier injection by forward bias, electrons and holes can also be generated by band gap light directed onto the top surface of the device. Uniform generation of high concentration of electrons and holes can be achieved in this case so that (3.5) becomes independent of position in the transition region. This is the simplest situation for interpretation of experimental data.

Although there will also be some absorption at the impurity centers and hence optical excitation of trapped electrons and holes by the band gap light, this is very small compared with interband optical absorption. As a consequence, if N, $P \gg N_D$ in the P^+N case, then $N = P$ and they are entirely determined by the interband optical absorption. For example, at $\hbar\omega = 1.8$ eV, the interband optical absorption coefficient in Si is about 10^3/cm while that of the impurity center is about

$$\alpha_n{}^0 = \sigma_n{}^0 n_T \simeq 10^{-17}\ \text{cm}^2 \times 10^{15}/\text{cm}^3 = 10^{-2}/\text{cm}$$

so that impurity absorption can be entirely

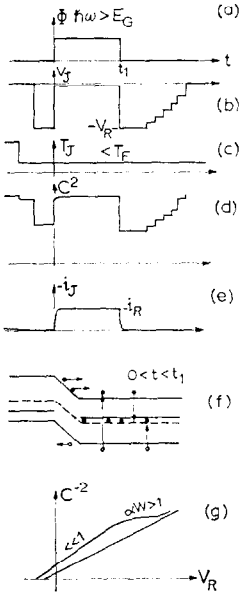

FIG. 7. The low temperature dark experiments with carrier generation by interband light.

neglected. This can also be demonstrated more quantitatively for the experimental conditions shown in Fig. 7(a), (b) and (c). During the time when interband light is turned on, $0 < t < t_1$ shown in Fig. 7(a), a reverse bias is applied to the diode through a limiting resistance R_L. The junction current is then $I_R = V_R/R_L$, as shown in Fig. 7(e). There is essentially no voltage drop across the diode or junction if optical generation is very high so that $P = N \gg N_E$. The steady state solution is $J_R = I_R/A = J_p + J_N =$ independent of position where

$$q^{-1}\,\mathrm{d}J_N/\mathrm{d}x = -q^{-1}\,\mathrm{d}J_p/\mathrm{d}x = N_{TT}[(c_n^t c_p^t PN - e_p e_n)/(c_n^t N + e_n + c_p^t P + e_p)] - G_I \qquad (3.6)$$

and

$$N_T/N_{TT} = (c_n^t N + e_p)/(c_n^t N + e_n + c_p^t P + e_p) \qquad (3.7)$$

where

$$e_n = e_n^t + e_n^0 \doteq e_n^0 = \sigma_n^0 \Phi$$

and

$$e_p = e_p^t + e_p^0 \doteq e_p^0 = \sigma_p^0 \Phi$$

when $T < T_F$ and $G_I = \alpha_I \Phi$ is the optical interband generation rate with a light flux of $\Phi(\hbar\omega > E_G)$ (in photon/cm^2-sec). For very high generation rate so that P and N are large, then one can show that $N \doteq P$ and $c_n^t N$, $c_p^t P \gg e_p^0$ and e_n^0. Thus, the trapped electron concentration given by (3.7) simplifies to

$$N_T/N_{TT} = c_n^t/(c_n^t + c_p^t) = n_T(0)/N_{TT} \qquad (3.7A)$$

which is also the trapped electron concentration in $0 < x < W$ as indicated above after the light is switched off at t_1 since the switch-off current transient contains only the very fast swept-out component and negligible carrier recombination would occur during this time. This initial condition would then give a N_I in the high frequency capacitance (3.1) which depends on c_n^t/c_p^t.

The squared capacitance ratio with and without light is then given by

$$[C/C_0]^2 = N_I(\text{light})/N_I(\text{dark}) \qquad (3.8)$$

Using Table 2 for the dark case and (3.7A) for the illuminated case, this ratio is obtained for the four examples of a single level center and tabulated in Table 3. It is evident that if the ratio N_{TT}/N_D or N_{TT}/N_A is determined from some other experiments such as experiment 1, then the capture ratio, c_n^t/c_p^t, can be determined from this experiment.

For low light levels such that the condition $N \doteq P \gg N_D$ does not hold in the P^+N structure, then $N_T = N_T(x)$ due to $P = P(x)$ and $N = N(x)$. Thus, C^{-2} vs. V_R would be nonlinear. An

Table 3. $(C/C_0)^2 - 1$ [*Equation* (3.8)]

	P^+N	N^+P
Donor	$(N_{TT}/N_D)(1 + c_n^t/c_p^t)$	$[N_{TT}/(N_A - N_{TT})](1 + c_p^t/c_n^t)$
Acceptor	$[N_{TT}/(N_D - N_{TT})](1 + c_n^t/c_p^t)$	$(N_{TT}/N_A)(1 + c_p^t/c_n^t)$

intermediate case where α_I is very large so that $\alpha_I W \gg 1$ for large V_R is illustrated in Fig. 7(g). The particular case corresponds to an acceptor center in a P^+N diode where $N_I(\text{dark}) = N_D - N_{TT} < N_I(\text{light}) = N_D - N_{TT}c_n^t/(c_n^t + c_p^t)$.

The interband optical generation experiment can be extended to higher photon energies so that the absorption is very strong and hence occurs only in the surface layer. The generated carriers would then be swept through the transition region by the large electric field at the limiting velocity. Some of these will be captured and cause an exponential increase of n_T or p_T in the transition region. A similar method was used for surface barrier diodes on GaAs by WILLIAMS.[13]

The temporal sequence is slightly different than those just discussed in Fig. 7. In this case, a large reverse bias is applied to the sample which appears across the junction at all times as indicated in Fig. 8(b). This is achieved by minimizing series resistance and removing the load resistance R_L used in the experiment shown in Fig. 7. Due to the high photon energy, carrier generation is very high near the surface layer and essentially negligible in the transition region. This is illustrated in Fig. 8(g) for the P^+N junction case where interband optical generation occurs in the thin P^+ surface layer. Electrons will be swept through the depletion region $0 < x < W$ by the large field and some of these will be captured by the unoccupied impurity centers. Thus,

$$dn_T/dt = c_n^t n(N_{TT} - n_T) \qquad 0 < x < W \qquad (3.9)$$

The electron concentration is essentially constant if the capture rate is small and the interband optical generation rate is high. Its value can be obtained from the steady state photocurrent, sketched in Fig. 8(f), and is $n \doteq N$ where

$$I = qv_s NA \qquad (3.10)$$

where v_s is the limiting velocity of the electrons in the high field region and A is the junction area. Thus, the solution of (3.9) is

$$n_T(t) = N_{TT} + N_{TT}[e_n^t/(e_n^t + e_p^t)] \exp(-t/\tau) \qquad (3.11)$$

where

$$\tau = 1/c_n^t N = qv_s A/I\sigma_n^t v_n \qquad (3.12)$$

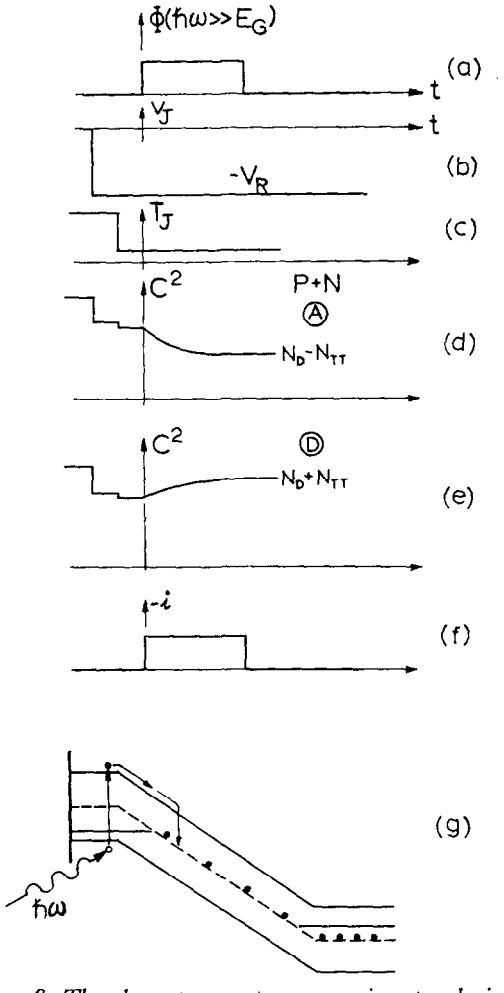

FIG. 8. The low temperature experiments during carrier generation by interband light at one surface, $\hbar\omega \gg E_G$. (a) light flux, (b) junction voltage, (c) junction temperature, (d) and (e) C^2 for P^+N junction with single level acceptor center and donor center respectively, (f) current, (g) band diagram showing optical generation at surface of P^+ layer.

σ_n^t is the capture cross section and v_n is the thermal velocity. In the high field region, $v_s \doteq v_n$ and σ_n^t is then defined as the capture cross section for hot electrons.

It is evident that interband optical generation can also be achieved in the N-type region of the P^+N structure if the N-type region is relatively thin. In this case, holes will be swept across the transition region and hole capture rate c_p^t can be

determined. If $e_n{}^t/e_p{}^t$ is large, then the initial condition should be that of t_0 shown in Fig. 4(b) so that most of the centers are occupied, and appreciable signal can be obtained.

Measurements of the capacitance transient using the experimental condition shown in Fig. 8 have been made for both P^+N and N^+P gold doped Si diodes. The data of the P^+N device used in Fig. 5(a) and (b) are given in Fig. 9(a). The data of all three photocurrent levels give an electron

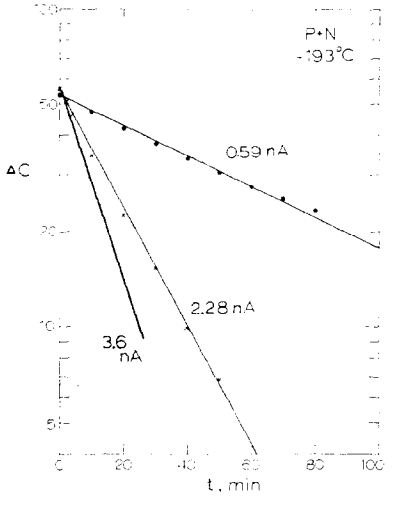

(a)

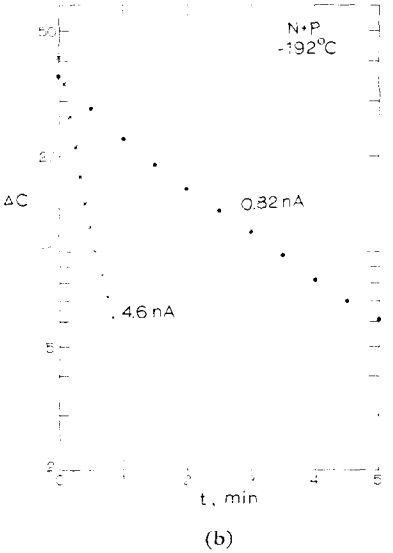

(b)

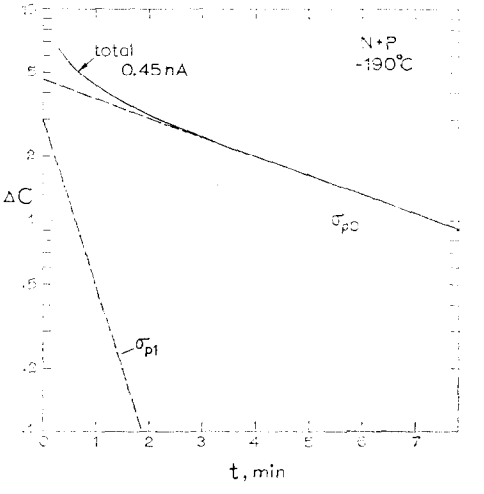

(c)

FIG. 9. Capacitance transient during surface optical excitation. (a) P^+N junction of Fig. 5, with electron captured by the neutral gold charge state, (b) N^+P junction with hole captured by the neutral gold charge state, (c) N^+P junction with the first hole captured by the acceptor gold charge state and the second hole captured by the neutral gold charge state, showing two time constents.

capture cross section at the neutral gold center of $\sigma_{n0}{}^t = qA/qI = 2.0\times10^{-16}$ cm^2 at 80°K.

For the N^+P case, the exponential decay of the junction capacitance depends on the initial condition of gold since gold can capture two holes if it is initially in the acceptor state and one hole if initially in the neutral state. The data of Fig. 9(b) corresponds to biasing the junction at 80°K with 2.3 μ illumination ($\hbar\omega = 0.54$ eV $E_D - E_V = 0.35$ eV) concurrently so that all of the gold atoms in $0 < x < W$ are in the neutral charge state initially. Then, holes are injected into the transition region by interband optical generation at the surface and captured by the neutral gold centers. The data at several steady state photocurrent levels give $\sigma_{p0}{}^t = (5.0\pm0.3)\times10^{-15}$ cm^2.

The data of Fig. 9(c) was obtained with most of the gold atoms in $0 < x < W$ in the acceptor charge state initially. This was achieved by valence band to impurity level optical excitation at 1.4 μ (0.88 eV). The decay of the capacitance shows two time constants. The initial fast transient comes from hole capture into the negatively charged gold acceptor state while the longer time constant from

the capture of holes into the neutral gold state. An analysis of the decay curve in Fig. 9(c) gives $\sigma_{p0}{}^{t} \simeq 5.0\times10^{-15}$ cm^2, in agreement with that obtained above, and $\sigma_{p1}{}^{t} = 5.5\times10^{-14}$ cm^2. This large value of hole capture cross section by a negatively charged gold acceptor state is consistent with the attractive Coulomb center model.

These preliminary results of capture cross sections are considerably different from those obtained by DAVIS[14] using alpha particle bombardment to generate electron–hole pairs in *PIN* structure and using the pulse height data together with a separate determination of the gold concentration. The present method is more accurate since it is independent of the gold concentration.

4. HIGH TEMPERATURE DARK CAPACITANCE AND CURRENT TRANSIENT EXPERIMENTS

In this section, we shall discuss the experiment similar to those in Section 3 but performed at sufficiently high temperatures so that the thermal emission rates, $e_n{}^{t}$ and $e_p{}^{t}$, are comparable to the measurement times involved. For these more general cases, one can obtain not only the C–V data at $t = 0+$ after the fast transients have passed as given in Section 3 but also the temporal variation of $C(t)$ and $i(t)$. The time constants will give the emission and capture rates and serve as direct measurements of these quantities and as redundant check for them obtained by other experiments. We shall again consider the three cases: no carrier injection, carrier injection by forward bias and carrier generation by interband light. These are experiments 4, 5 and 6 listed in Table 1. In addition to the electrical turn-on transient, the electrical turn-off transient will also provide additional data for the determination of the thermal capture rates, $c_n{}^{t}$ and $c_p{}^{t}$.

4.1 *Experiments* 4, *no carrier injection*

The temporal variation of the parameters for this experiment are shown in Fig. 10(a), (b) and (c). The expected capacitance and current transients

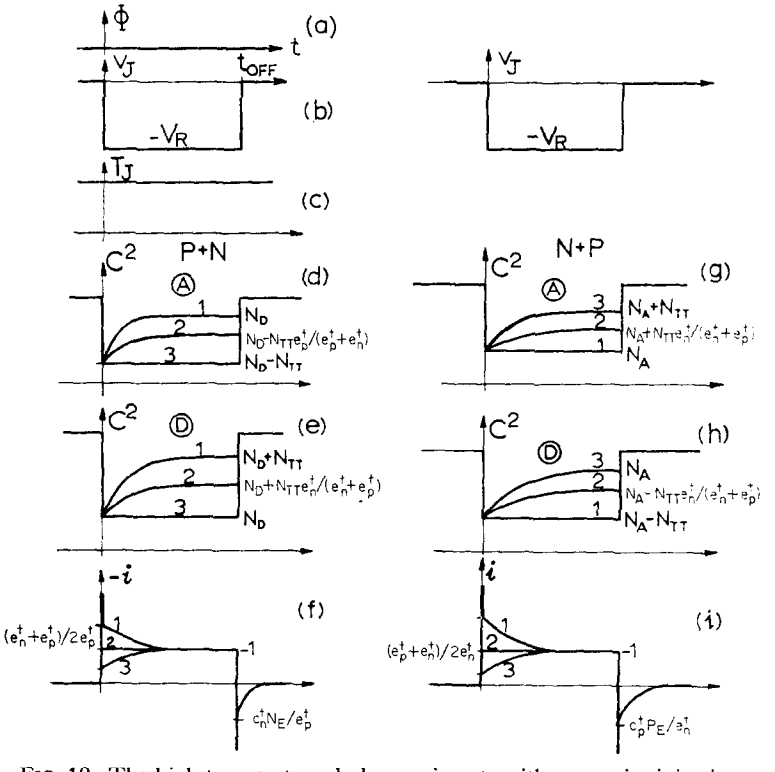

FIG. 10. The high temperature dark experiments with no carrier injection.

for the P^+N and N^+P junctions are shown in Fig. 10(d–i) for either a one-level donor or acceptor center. The complete expressions of the capacitance and current transients are derived below.

Making use of the depletion assumption, $n = p = 0$, in the transition region after the junction voltage is switched from $V = 0$ to $V = -V_R$, the trapped electron concentration from (2.1C) is given by

$$n_T(t) = n_T(\infty) + [n_T(0) - n_T(\infty)] \exp(-t/\tau_{ON}) \qquad 0 < x < W \qquad (4.1)$$

where

$$n_T(0) = N_{TT}[N_E/(N_E + n_1)] \qquad (4.2)$$

$$\doteq N_{TT} \qquad (P+N \text{ junction}) \qquad (4.2A)$$

$$\doteq 0 \qquad (N+P \text{ junction}) \qquad (4.2B)$$

$$n_T(\infty) = N_{TT}[e_p{}^t/(e_n{}^t + e_p{}^t)] \qquad (4.3)$$

and

$$\tau_{ON} = 1/(e_n{}^t + e_p{}^t) \qquad (4.4)$$

The capacitance transient is then given by

$$C^2(t) = qN_I(t)/2K_s\epsilon_0(V_D + V_R) \qquad 0 < t < t_{OFF} \qquad (4.5)$$

for spatially independent N_I. The relationships between $N_I(t)$, N_D, N_A, $n_T(t)$ and $p_T(t)$ in P^+N and N^+P structures for acceptor-like and donor-like centers are listed in Table 4. The initial and

Table 4. $N_I(t)$

		Junction structure	
		P^+N	P^+N
Defect type	Donor	$N_D + p_T$	$N_A - p_T$
	Acceptor	$N_D - n_T$	$N_A + n_T$

final values of the square of the junction capacitance given by (4.5) and illustrated in Fig. 10(d), (e), (g) and (h) can be readily obtained using this table. For example, for a donor center in the P^+N junction as illustrated in Fig. 10(e), the initial value is

$$C^2(0+) \propto N_I(0+) = N_D + p_T(t) = N_D + N_{TT} \times [n_1/(N_E + n_1)] \doteq N_D$$

where

$$p_T(0+) = N_{TT} - n_T(0+) \doteq 0$$

is obtained from (4.2A). The final value of the capacitance squared prior to turn-off of the reverse bias is

$$C^2(t = t_{OFF} \gg \tau_{ON}) \propto N_I(\infty) = N_D + p_T(\infty) = N_D + N_{TT}[e_n{}^t/(e_n{}^t + e_p{}^t)].$$

Thus, for case (3) labeled in Fig. 10(e) where $e_p{}^t \gg e_n{}^t$, $C(\infty) = C(0+)$ and there is no capacitance change while for case (1) where $e_p{}^t \ll e_n{}^t$, the capacitance change is maximum and is given by $C(\infty)/C(0+) = \sqrt{[(N_D + N_{TT})/N_D]}$. An inspection of the results given in Fig. 10(d), (e), (g) and (h) shows that the ratio $[C(\infty)/C(0+)]^2$ allows an accurate determination of the ratio $e_n{}^t/e_p{}^t$ and the nature of the defect center (acceptor- or donor-like), if the total defect concentration N_{TT} is determined by some other methods such as that described in Section 3.1. Generally, a very small change of capacitance can be readily detected so that this method can also be used for either very large or very small ratios of $e_n{}^t/e_p{}^t$. The result of this ratio can then be combined with the measurement of the time constant $\tau_{ON} = 1/(e_n{}^t + e_p{}^t)$ to give the values of $e_n{}^t$ and $e_p{}^t$ separately.

If the impurity concentration varies spatially, the solution of the capacitance is quite complex so that simple interpretation is not possible, however, the decay time constant still gives $\tau_{ON} = 1/(e_n{}^t + e_p{}^t)$. For this case, the low temperature experiments in Section 3.1 are most useful.

The current transient during the turn-on phase contains a fast component indicated by the spike shown in Fig. 10(f) and (i). This is due to the sweep-out of the majority carriers present in the region $W_0 < x < W$ prior to reversing the applied voltage, indicated in Fig. 11(a) and (b). This current pulse is similar to that shown in Fig. 4(f) and will decay in approximately the transit time across the high field region W with limiting velocity of 10^7 cm/sec. This is of the order of 10^{-11} to 10^{-10} sec. If the circuit limits

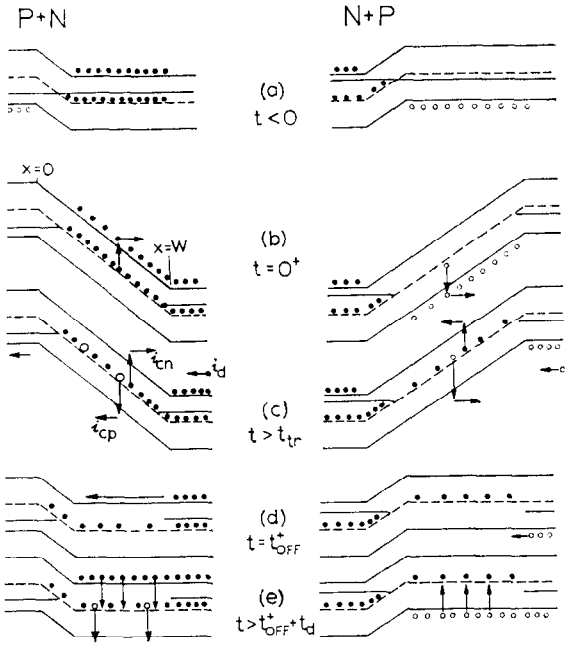

FIG. 11. The energy bands during the switching transients of the high temperature dark experiments shown in Fig. 10. Figure (c) shows the two components of the turn-on current and Fig. (e) shows the recombination current during turn-off phase.

the junction current, then this fast pulse will have a width of approximately

$$qN_I(W-W_0)A/I_R \doteq 10^{-8} \text{ sec}$$

if

$$N_I = 10^{15}/\text{cm}^3, \quad W-W_0 = 10^{-4} \text{ cm},$$
$$A = 10^{-4} \text{ cm}^2 \quad \text{and} \quad I_R = 1 \text{ mA}.$$

The slow current transient consists of three parts as indicated in Fig. 11(c): The electron and hole conduction or generation currents, i_{cn} and i_{cp}, and the displacement current, i_d, due to the induced charges in the quasi-neutral regions, $x < 0$ and $x > W$, by the time dependence of the trapped charge n_T. The total current can be obtained at the plane $x = W$. The conduction current here is entirely due to electrons and is given by

$$i_{cn}(t) = A\int_0^W q(\mathrm{d}n/\mathrm{d}t)_T \,\mathrm{d}x \tag{4.6}$$

$$= qe_n^t n_T(t) W(t) A \qquad [n_T \neq f(x)] \tag{4.6A}$$

where in (4.6A) spatially constant N_I is assumed and (2.1A) is used for $(\mathrm{d}n/\mathrm{d}t)_T$ with $n = 0$. The lower limit of integration should be W_0 and a different set of $n_T(t)$ should be used in $0 < x < W_0$ due to different initial condition here from that in $W_0 < x < W$ as indicated in Fig. 11(a). For simplicity, this is neglected. The time dependence of $W(t)$ comes from $N_I(t)$ or $n_T(t)$ as indicated in Table 4 and (4.1) to (4.3).

The induced or displacement current at $x = W$ can be computed readily for the one-dimensional model, using the time rate of change of the charge induced by $n_T(t)$ at $x = W$. This is

$$i_d(t) = A\int_0^W q(\mathrm{d}n_T/\mathrm{d}t)(x/W)\,\mathrm{d}x \tag{4.7}$$

$$= (qWA/2)(\mathrm{d}n_T/\mathrm{d}t) \qquad [n_T \neq f(x)] \tag{4.7A}$$

The total junction current from the sum of (4.6) and 4.7) is then

$$i(t) = qA\int_0^W \{(x/W)e_p^t p_T + [(W-x)/W]e_n^t n_T\}\,\mathrm{d}x \tag{4.8}$$

$$= (qWA/2)(e_p^t p_T + e_n^t n_T) \qquad [n_T = N_{TT} - p_T \neq f(x)] \tag{4.8A}$$

which is not truly exponential since

$$W = W(t) = \sqrt{[2K_s\epsilon_0(V_D+V_R)/qN_I(t)]}.$$

The initial value is

$$i(0+) = (qW_0AN_{TT}/2)e_n^t \qquad (P^+N \text{ junction}) \tag{4.9A}$$

$$= (qW_0AN_{TT}/2)e_p^t \qquad (N^+P \text{ junction}) \tag{4.9B}$$

where use is made of (4.2A) and (4.2B) in (4.8) respectively for the two structures. The final current is just the steady state dark current, which from (4.8) using (4.3) is given by

$$i(\infty) = qW_\infty AN_{TT}[e_n^t e_p^t/(e_n^t + e_p^t)] \tag{4.10}$$

Thus, the ratio of the initial and final dark currents is given by

$$i(0+)/i(\infty) = (1/2)(1+e_n{}^t/e_p{}^t)(W_0/W_\infty) \quad (P^+N \text{ junction}) \quad (4.11A)$$

$$= (1/2)(1+e_p{}^t/e_n{}^t)(W_0/W_\infty) \quad (N^+P \text{ junction}) \quad (4.11B)$$

The factor (W_0/W_∞) can be obtained from $W(t) = \sqrt{[2K_s\epsilon_0(V_D+V_R)/qN_I(t)]}$, the relationships given in Table 3 and the initial and final values of $n_T(t)$ given by (4.2A), (4.2B) and (4.3). These ratios are tabulated in Table 5.

has passed in a time of the order of the dielectric relaxation time of the majority carriers, $t_d = K_s\epsilon_0/q\mu_n N_E \doteq 10^{-12}$ sec. We move the time scale reference to $t = t_{\text{OFF}}$, thus the initial condition for the turn-off transient is

$$n_T(0+t_{\text{OFF}}) = n_T(\infty) = N_{TT}[e_p{}^t/(e_n{}^t+e_p{}^t)] \quad (4.12)$$

and the final value or the equilibrium value is given by (4.2A) and (4.2B):

$$n_T(\infty+t_{\text{OFF}}) = N_{TT}[N_E/(N_E+n_1)] \doteq N_{TT} \ (P^+N \text{ junction}) \quad (4.13A)$$

$$\doteq 0 \ (N^+P \text{ junction}) \quad (4.13B)$$

Table 5 The ratio $[W_0/W_\infty]^2 - 1 = [N_I(\infty)/N_I(0)] - 1$

	P^+N	N^+P
Donor	$(N_{TT}/N_D)[e_n{}^t/(e_n{}^t+e_p{}^t)]$	$[N_{TT}/(N_A-N_{TT})][e_p{}^t/(e_n{}^t+e_p{}^t)]$
Acceptor	$[N_{TT}/(N_D-N_{TT})][e_n{}^t/(e_n{}^t+e_p{}^t)]$	$(N_{TT}/N_A)[e_p{}^t/(e_n{}^t+e_p{}^t)]$

The current ratios given by (4.11A) and (4.11B) are very useful since they allow the determination of the ratio $e_n{}^t/e_p{}^t$ directly if N_{TT}/N_D or N_{TT}/N_A is small or is known from other experiments such as that in Section 3.1. In addition, the decay data also gives the time constant $\tau_{\text{ON}} = 1/(e_n{}^t+e_p{}^t)$ so that both $e_n{}^t$ and $e_p{}^t$ can be uniquely determined. The most convenient structures are evidently those with $N_{TT} \ll N_D$ or $N_{TT} \ll N_A$ since then $e_n{}^t$ and $e_p{}^t$ can be determined entirely from the dark current transient without additional experiments. However, electric field dependences of $e_n{}^t$ and $e_p{}^t$ will complicate the interpretation.[5,6,8,15-17]

The junction current transients during electrical turn-on phase just described are summarized in Fig. 10(f) and (i). Cases labeled (2) in these figures correspond to $e_n{}^t = e_p{}^t$ which have only an initial fast decay due to sweep-out of majority carriers.

The electrical turn-off current transients indicated in Fig. 10(f) and (i) will provide additional data of capture coefficients. The junction current expression is worked out below for the slower turn-off transient indicated in Fig. 11(e) after the fast initial turn-off transient indicated in Fig. 11(d) We shall assume that during the turn-off phase, the electron concentration in the region $W_0 < x < W$ is essentially equal to the equilibrium value as illustrated in Fig. 11(e) and the hole concentration is negligible. Then an exponential time dependent solution of (2.1C) can readily be obtained giving

$$n_T(t+t_{\text{OFF}}) = n_T(\infty+t_{\text{OFF}}) + [n_T(0+t_{\text{OFF}}) - n_T(\infty+t_{\text{OFF}})]\exp(-t/\tau_{\text{OFF}}) \quad (4.14)$$

where the initial and final values are given by (4.12), (4.13A) and (4.13B) and

$$\tau_{\text{OFF}} = 1/(c_n{}^tN_E + e_n{}^t + c_p{}^tP_E + e_p{}^t) \doteq 1/c_n{}^tN_E (P^+N \text{ junction}) \quad (4.15A)$$

$$\doteq 1/c_p{}^tP_E (N^+P \text{ junction}) \quad (4.15B)$$

The turn-off current transient after the initial fast turn-off transient comes from the net recombination over generation in $0 < x < W$ since $n_T(t)$ is not at its equilibrium value and nor are $n(x)$ and $p(x)$. These must approach the equilibrium value at $t = \infty$. Using the approximation of

$n \doteq N_E$ and $p \doteq P_E$, then the total current is given by

$$i_J(t+t_{OFF}) = qA\int_0^W (dn_T/dt)dx \simeq qAW(dn_T/dt)$$
$$= qAW[(c_n^t N_E + e_p^t)p_T(t) - (c_p^t P_E + e_n^t)n_T(t)] \quad (4.16)$$

where use is made of (2.1C). From the solution of $n_T(t)$ and $p_T(t)$ given by (4.14), the turn-off junction current after the initial fast transient becomes

$$i_J(t+t_{OFF}) = qWAN_{TT}[(c_n^t N_E e_n^t - c_p^t P_E e_p^t)/(e_n^t + e_p^t)]\exp(-t/\tau_{OFF}) \quad (4.17)$$

For $P+N$ junction where $N_E \gg n_1, p_1, p_E$ so that

$$i_J(t+t_{OFF}) = qWAN_{TT}[c_n^t N_E e_n^t/(e_n^t + e_p^t)] \times \exp(-c_n^t N_E t) \quad (4.18)$$

and for $N+P$ junctions where $P_E \gg p_1, n_1, N_E$, then

$$i_J(t+t_{OFF}) = -qWAN_{TT}[c_p^t P_E e_p^t/(e_p^t + e_n^t)] \times \exp(-c_p^t P_E t) \quad (4.19)$$

These results again suggest that the current ratios can provide capture to emission rate ratios from experimental data without the knowledge of $qWAN_{TT}$. Thus, at the start of the turn-off transient, but after the fast spike, the junction currents for the two diodes are

$$i_J(0_{OFF}) = qWAN_{TT}[c_n^t N_E e_n^t/(e_n^t + e_p^t)] \quad (P^+N) \quad (4.20A)$$

and

$$i_J(0_{OFF}) = -qWAN_{TT}[c_p^t P_E e_p^t/(e_n^t + e_p^t)] \quad (N^+P) \quad (4.20B)$$

Taking the ratio with the dark current for $V = -V_R$ given by (4.10), then

$$|i_J(0_{OFF})/i_J(\infty)| = c_n^t N_E/e_p^t \quad (P^+N) \quad (4.21A)$$
$$= c_p^t P_E/e_n^t \quad (N^+P) \quad (4.21B)$$

Thus, using the turn-on transient to get e_n^t and e_p^t, the capacitance data to get N_E and P_E, the capture rates c_n^t and c_p^t can be determined. This also provides a self-consistent check since the capture rates can also be determined from the time constant of the decay curve of the turn-off current as indicated by (4.15A) and (4.15B).

Experimental data of capacitance and current transients are obtained for the P^+N gold doped silicon diode shown in Fig. 5(a). The capacitance data was taken at $-65.1°C$ while the current data

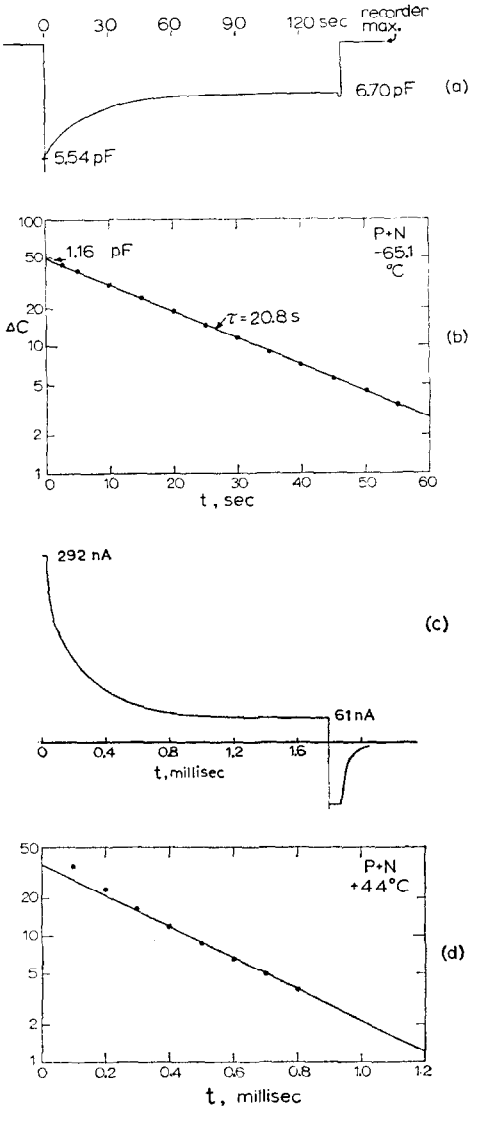

FIG. 12. The experimental data of gold doped P^+N Si diode of Fig. 5. (a) actual recorder trace of capacitance transient, (b) ΔC of (a), (c) recorder trace of current transient and (d) Δi of (c).

was taken at +44°C. These are shown in Fig. 12(a) to (d).

The capacitance transient in Fig. 12(a) shows the feature predicted by curve (1) of Fig. 10(d) and $\Delta C(t)$ is truly exponential as indicated in Fig. 12(b). The data is taken at $V_R = 36$ V. From the initial and final capacitance values obtained from Fig. 12(b) and (a) respectively, we have

$$[C(\infty)/C(0)]^2 = (6.70/5.45)^2 = 1.465$$
$$= [1-(N_{TT}/N_D)e_p^t/(e_n^t+e_p^t)]/[1-(N_{TT}/N_D)]$$

so that

$$N_{TT}/N_D = 0.465/[1.465-e_p^t/(e_n^t+e_p^t)].$$

This ratio is essentially identical to those from the experiments shown in Fig. 5(a) which gave

$$N_{TT}/N_D = 0.464/[1.464-e_p^t/(e_n^t+e_p^t)].$$

This results shows further that either e_p^t/e_n^t is entirely independent of temperature since Fig. 5(a) gives the ratio at 300°K while the present experiment is performed at −65.1°C, or the results imply $e_p^t/e_n^t \ll 1$. The data on the control diode shown in Fig. 5(a) was used to demonstrate that $e_p^t \ll e_n^t$ is the correct situation. The decay time constant of the ΔC vs. t plot in Fig. 12(b) also gives the sum $e_n^t+e_p^t = 1/\tau = 1/20.8 = 0.0482$/sec for the acceptor gold level in silicon.

The junction current transient shown in Fig. 12(c) and (d) can be used to obtain the values of e_p^t and e_n^t as indicated by (4.11A). From Table 5 for the P^+N structure with the gold acceptor center, we have

$$W_0/W_\infty = \sqrt{[1+N_{TT}e_n^t/(N_{TT}-N_D)(e_p^t+e_n^t)]}$$
$$\doteq \sqrt{[1+N_{TT}/(N_{TT}-N_D)]}$$

for $e_p^t/e_n^t \ll 1$. Using the data of Fig. 5(a) with this approximation, then

$$W_0/W_\infty \doteq \sqrt{(1.465)} = 1.21.$$

The ratio of the initial and final current can be obtained from Fig. 12(c) and (d) and is

$$i(0)/i(\infty) = 292 \text{ nA}/61 \text{ nA} = 4.80.$$

Using (4.11A), then

$$e_n^t/e_p^t = 2[i(0)/i(\infty)][W_\infty/W_0]-1 = 6.9.$$

This first estimate is already quite accurate and may be used to calculate the value of N_D and N_{TT} from the data of Fig. 5(a) at 23°C rather than 44°C of the present experiment since the ratio e_p^t/e_n^t is not very sensitive to temperature. Thus, from $N_{TT}e_n^t/(e_n^t+e_p^t) = 2.88\times10^{14}/\text{cm}^3$ and $N_D-N_{TT} = 6.22\times10^{14}/\text{cm}^3$ obtained in Fig. 5(a), we have $N_{TT} = 4.15\times10^{14}/\text{cm}^3$ and $N_D = 1.04\times10^{15}/\text{cm}^3$. The donor concentration is in excellent agreement with the value obtained from the starting resistivity of the substrate, $N_D = 1\times10^{15}/\text{cm}^3$, and the gold concentration is consistent with the gold diffusion schedule discussed previously in Section 3.3.

The values of the thermal emission rate at 44°C can be obtained from the result of the ratio given above and the decay time constant of the junction current. From Fig. 12(d), we have $e_n^t+e_p^t = 1/\tau = 1/345\,\mu$sec, giving $e_n^t = 1/396\,\mu\text{sec} = 2520$/sec and $e_p^t = 1/2730\,\mu\text{sec} = 365$/sec. These values are in excellent agreement with those obtained from the photocurrent transients described in Section 6 and with other experiments such as the generation–recombination noise spectra[17] and the pulsed field effect transient.[16]

The slight nonexponential dependence of $\Delta i(t)$ shown in Fig. 12(d) comes from the effect of $W(t)$ due to high N_{TT}. This effect is expected from the result of $W_0/W_\infty = 1.2$ obtained above, which accounts for the fast initial drop of $i(t)$.

4.2 *Experiments* 5, *carrier injection by forward bias*

The experimental condition here is identical to that of Experiment 2 described in Section 3.2 except that the junction temperature is above the freeze-out temperature so that the thermal emission rates are appreciable. Thus, when the junction voltage is switched from $+V_F$ to $-V_R$, the trapped electron concentration is given by (3.5) and is position dependent due to the injected electrons (N^+P case) or holes (P^+N case) as discussed in Section 3.2. If high injection level is achieved so that $N \doteq P \gg N_E$ or P_E in $0 < x < W$ after the initial transients described in Fig. 6(d) have passed, then the initial condition for the slow transient is

$$n_T(0) = N_{TT}e_n^t/(e_n^t+e_p^t) \qquad (4.22)$$

This would then replace (4.2) and all the other results apply, such as (4.1) to (4.8).

The square of the initial and final capacitance ratio can be readily obtained from (4.5) using the initial and final values of n_T. These are

P^+N: Acceptor center $[1-(N_{TT}/N_D)c_n^t/(c_n^t+c_p^t)]/[1-(N_{TT}/N_D)e_p^t/(e_n^t+e_p^t)]$ (4.23A)

Donor center $[1+(N_{TT}/N_D)c_p^t/(c_n^t+c_p^t)]/[1+(N_{TT}/N_D)e_n^t/(e_n^t+e_p^t)]$ (4.23B)

N^+P Acceptor center $[1+(N_{TT}/N_A)c_n^t/(c_n^t+c_p^t)]/[1+(N_{TT}/N_A)e_p^t/(e_n^t+e_p^t)]$ (4.24A)

Donor center $[1-(N_{TT}/N_A)c_p^t/(c_n^t+c_p^t)]/[1-(N_{TT}/N_A)e_n^t/(e_n^t+e_p^t)]$ (4.24B)

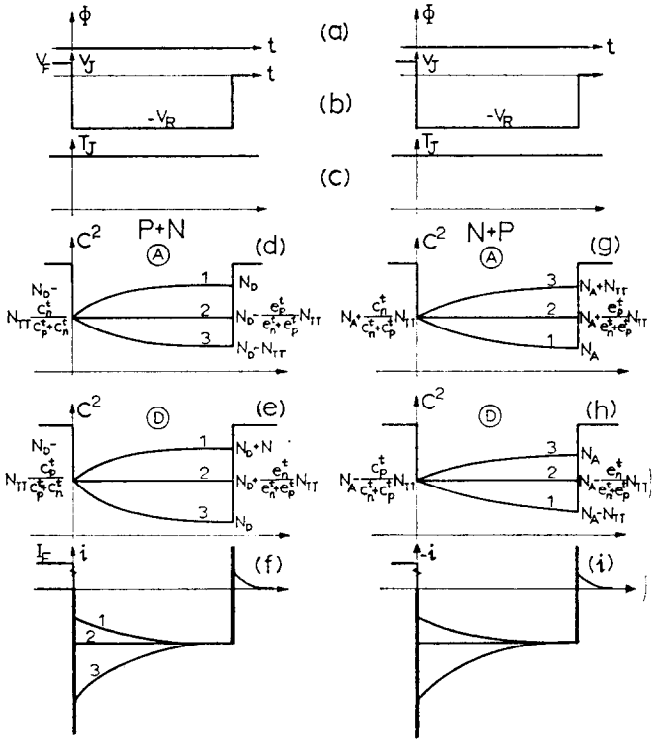

FIG. 13. The high temperature dark experiments with carrier injection by forward bias the junction.

The capacitance transients for these four cases are graphed in Fig. 13(d), (e), (g) and (h) which show that the capacitance can either increase or decrease while the zero injection case can have only increasing or constant capacitance as illustrated in Fig. 10(d), (e), (g) and (h).

The three cases labeled (1), (2) and (3) in Fig. 13(d), (e), (g) and (h) correspond to

(1) $(e_n^t/e_p^t) > (c_p^t/c_n^t)$ or $p^* > n^*$ (4.25A)

(2) $(e_n^t/e_p^t) = (c_p^t/c_n^t)$ or $p^* = n^* = n_i$ (4.25B)

(3) $(e_n^t/e_p^t) < (c_p^t/c_n^t)$ or $p^* < n^*$ (4.25C)

where n^* and p^* are the equality electron and hole concentrations.[18] These results show that if both N_{TT}/N_D (or N_{TT}/N_A) and e_n^t/e_p^t have already been determined by other experiments, then the present experiment can provide a determination

of the ratio c_n^t/c_p^t by observing the capacitance transient.

The electrical turn-on dark reverse current transient contains a fast initial part identical to that shown in Fig. 6(d). This is shown as a negative spike at $t = 0$ in Fig. 13(f) and (i). The slow transient during $0 < t < t_R$ can be obtained from (4.8A) using (4.1), (4.3), (4.4) and (4.22). This is given by

$$i(t) = (qWAN_{TT}/2)([2e_n^t e_p^t/(e_n^t + e_p^t)] + \{[c_n^t/(c_n^t + c_p^t)] - [e_p^t/(e_n^t + e_p^t)]\} \times (e_n^t - e_p^t)\exp(-t/\tau_{ON})) \quad (4.26)$$

where

$$\tau_{ON} = 1/(e_n^t + e_p^t)$$

and

$$W = W(t) = \sqrt{[2K_s\epsilon_0(V_D + V_R)/qN_I(t)}$$

and $N_I(t)$ is given by Table 4. The ratio of the initial to final current is

$$i(0)/i(\infty) = \frac{1}{2}\left[\frac{1+(e_p^t/e_n^t)}{1+(c_n^t/c_p^t)} + \frac{1+(e_n^t/e_p^t)}{1+(c_p^t/c_n^t)}\right] \times (W_0/W_\infty) > \tfrac{1}{2} \quad (4.27)$$

where $W_0/W_\infty > 1$ is given in Table 5. The current transient here is again not a true exponential due to the time dependence of $W(t)$ and this is similar to the no injection case given by (4.8A). Approximate exponential decay is obtained if $N_{TT} \ll N_D$ or $N_{TT} \ll N_A$.

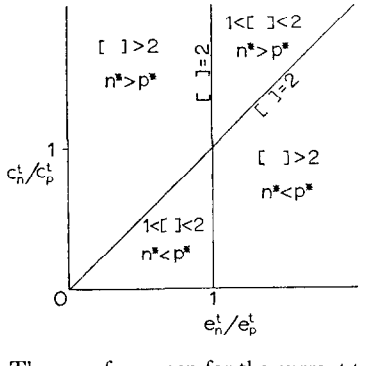

FIG. 14. The waveform map for the current transient of Fig. 13(f) and (i). [ ] is given by the bracket in (4.27).

The inequality predicted in (4.27), indicating the current ratio to be greater than 1/2 for all conditions, can be demonstrated by considering the factor in the bracket [ ]. This factor is always greater than 1 and a map is constructed in Fig. 14 giving the range of this factor as a function of e_n^t/e_p^t and c_p^t/c_n^t. The map is divided into four regions by two lines of [ ] = 2 which are $e_n^t/e_p^t = 1$ and $e_n^t/e_p^t = c_p^t/c_n^t$ or $p^* = n^* = n_i$.

The three types of decay curves shown in Fig. 13(f) and (i) correspond to the following conditions if N_{TT} is small so that $W_0 = W_\infty$.

(1) $(p^*/n^*) < 1 < (e_n^t/e_p^t)$ or $(p^*/n^*) > 1 > (e_n^t/e_p^t)$ (4.28A)

(2) $p^* = n^* = n_i$ or $e_n^t = e_p^t$ (4.28B)

(3) $(n^*/p^*) < 1 < (e_n^t/e_p^t)$ or $(n^*/p^*) > 1 > (e_n^t/e_p^t)$

The turn-off transient is identical to that in Section 4.1 without injection since the dark steady state condition of the applied bias $-V_R$ is reached at $t = t_R$.

4.3 *Experiments 6, carrier generation by interband light*

The experimental conditions are identical to those given by Experiments 3 discussed in Section 3.3, except that the junction temperature is high so that the thermal emission rates are no longer negligible. It is evident that the condition of high optical generation rate is the simplest for experimental data interpretation since then $N \doteq P \gg N_D$ or N_A so that the spatially constant initial condition for the trapped electron concentration given by (4.22) can be used. The results obtained in Section 4.2 can then be applied with $t = 0$ corresponding to the time when the light is switched off and the applied bias is $-V_R$ at all times prior to switching off at $t = t_R$.

This method of producing high concentration of carriers is preferred over that by forward bias since the carrier concentrations can be made very high over the entire transition region so that the condition (4.22) is very closely satisfied.

If photon energy is appreciably greater than the band gap, then the electron and hole pairs are generated in the surface layer as discussed in Fig. 8(g). For the high temperature case here,

thermal emission of electrons and holes may be important if the interband optical generation rate is small. Then (2.1C) must be considered instead of (3.9). The optical excitation from the impurity level can still be neglected so that the four emission and capture processes in (2.1C) are all due to thermal processes in the transition region. Thus,

$$\begin{aligned} dn_T/dt = & -(c_n{}^t N + e_n{}^t + c_p{}^t P + e_p{}^t) n_T \\ & + (c_n{}^t N + e_p{}^t) N_{TT}, \end{aligned} \tag{4.29}$$

where the electron and hole concentrations in the junction transition region $0 < x < W$ are determined by the steady state dark and photo currents. For the P^+N example with generation in the P^+ layer, then photoelectrons are swept across the transition region so that $N = \Delta N + N_0$ and $\Delta N = \Delta J/qv_s$ is the photoelectron concentration, ΔJ is the photocurrent density (per junction area) and N_0 is the dark electron concentration. The hole concentration in the transition region is just the dark value, $P = P_0$. The dark concentrations are small and can be obtained from the dark leakage current given by

$$J_{\text{dark}} = qWN_{TT}/\tau_0 = qv_s(N_0 + P_0)$$

or $(N_0 + P_0) = N_{TT}\tau_{tr}/\tau_0$ where $\tau_{tr} = W/v_s \doteq 10^{-11}$ sec is the transit time and $\tau_0 = (e_n{}^t + e_p{}^t)/e_n{}^t e_p{}^t > 10^{-3}$ sec is the average thermal emission rate. Thus, the simplest experimental condition for obtaining the capture rate directly is to have strong interband optical excitation. The explicit condition for the P^+N case just described can be obtained by rewriting (4.29) to give

$$\begin{aligned} dn_T/dt = & -c_n{}^t[N + n_1 + (c_p{}^t/c_n{}^t)P + n^*]n_T \\ & + (c_n N + e_p) N_{TT} \\ = & -c_n{}^t[N_0 + (\Delta J/qv_s) + n_1 + n^* \\ & + (c_p{}^t/c_n{}^t)P_0]n_T + (c_n N + e_p) N_{TT}. \end{aligned} \tag{4.30}$$

This shows that if the optical injection is sufficiently high so that $\Delta J/qv_s \gg N_0$, n_1, n^* and $(c_p{}^t/c_n{}^t)P_0$, then (3.9) is again applicable and the exponential decay time constant of n_T or the junction capacitance measures $c_n{}^t$ directly as given by (3.12). The time constant is less than the thermal emission rate (10^{-2} sec at 300°K for Au in Si) and may pose a practical problem of measuring the capacitance transient, $C(t)$.

5. LOW TEMPERATURE PHOTOCAPACITANCE AND PHOTOCURRENT EXPERIMENTS

These experiments are similar to those in Section 3, but with the addition of photoexcitation of electrons and holes trapped at the impurity centers by light with $E_G > \hbar\omega > E_C - E_T$ or $E_T - E_V$. In addition to the data of $e_n{}^t$, $e_p{}^t$, $c_n{}^t$ and $c_p{}^t$ and their ratios, the photocurrent and photocapacitance transients will also provide data of the optical emission rates and cross sections and their temperature, photon energy and electric field dependences. Three types of experiments, listed as 7, 8 and 9 in Table 1, are discussed below.

5.1 *Experiments 7, no carrier injection*

The experimental conditions are shown in Fig. 15(a), (b) and (c) and the photocapacitance and current waveforms in Fig. 13(e) to (i). The waveforms are identical to those shown in Fig. 10 (exp. 4) where electrons and holes are thermally excited from the impurity centers. Thus, the results of Section 4.1 can be carried over to these experiments if all $e_n{}^t$ and $e_p{}^t$ there are replaced by $e_n{}^0$ and $e_p{}^0$. The only difference is that there is no initial current spike here while they were present previously in Fig. 10(f) and (i).

One of the distinct advantages of this method over previous methods is the possibility of varying photon energy so that either $e_n{}^0$ or $e_p{}^0$ can be made zero by reducing the photon energy to below the threshold of either electron or hole emission respectively. For example, taking the P^+N gold doped Si as an illustration, then since $E_C - E_T = 0.54$ eV or $E_T - E_V = 0.62$ eV at 100°K, we can use $\hbar\omega = 0.58$ eV to get $e_n{}^0 > 0$ and $e_p{}^0 = 0$. Thus, the capacitance transient waveform is given by curve (1) of Fig. 15(d) and N_{TT} can be obtained directly, or $[C(0)/C(\infty)]^2 = 1 - (N_{TT}/N_D)$ gives N_{TT}/N_D. The time constant gives the emission rate: $e_n{}^0 = 1/\tau$. As the photon energy is increased to $\hbar\omega > E_T - E_V$, both optical emission of electrons and holes must be included to give $e_n{}^0 + e_p{}^0 = 1/\tau$ and

$$\begin{aligned} [C(0)/C(\infty)]^2 = & [1 - (N_{TT}/N_D)]/[1 - (N_{TT}/N_D) \\ & \times e_p{}^0/(e_p{}^0 + e_n{}^0)] \end{aligned}$$

as indicated by curve (2) of Fig. 15(d). Since N_{TT}/N_D was just obtained when $e_p{}^0 = 0$, the ratio $e_n{}^0/e_p{}^0$ can be obtained from this capacitance

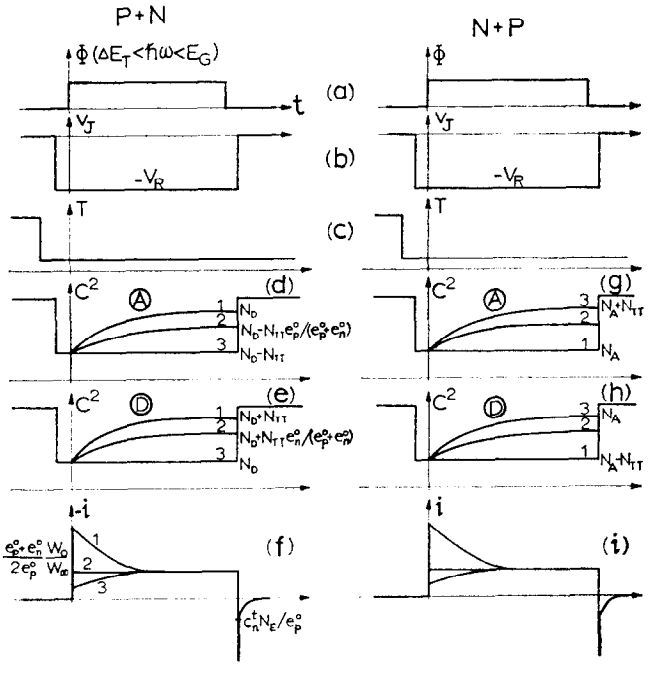

FIG. 15. Low temperature photoexperiments with no injection of carriers.

ratio. Explicitly, this ratio for the P^+N case with an acceptor center located above midgap is given by

$$(e_p^0/e_n^0)_\lambda = [C(0)/C(\infty)]_\lambda{}^2 - [1-(N_{TT}/N_D)] \quad (5.1\text{A})$$

$$= [C(0)/C(\infty)]_\lambda{}^2 - [C(0)/C(\infty)]_{\lambda+}{}^2, \quad (5.1\text{B})$$

where λ is the wavelength of the photon with $\hbar\omega > E_T - E_V$ while $\lambda+$ is the photon wavelength with $E_C - E_T < \hbar\omega < E_T - E_V$.

Extensive experimental data of the optical cross sections using this technique for both the gold acceptor level ($E_C - E_T = 0.54$ eV) and donor level ($E_T - E_V = 0.35$ eV) in Si have been obtained by Forbes which will be reported in a subsequent

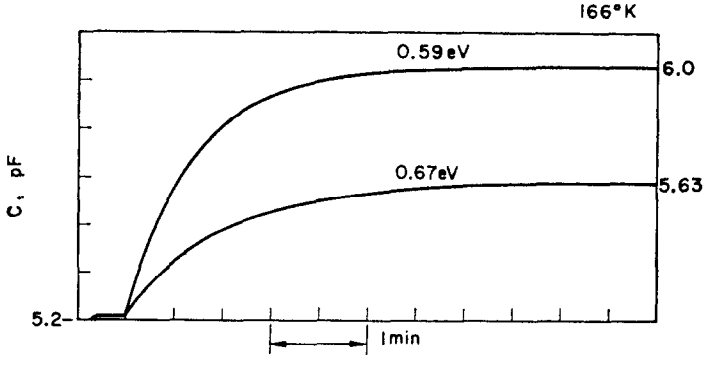

FIG. 16. The capacitance transient of the P^+N diode of Fig. 5 at two photon energies, 0.59 eV and 0.67 eV, illustrating $e_p{}^0 = 0$ for the 0.59 eV condition.

paper. For a demonstration, the data at 166°K of a P^+N gold doped Si diode is shown in Fig. 16. The upper capacitance curve shows optical excitation from the acceptor level ($E_C - E_T = 0.54$ eV and $E_T - E_V = 0.60$ eV) to the conduction band and the lower curve shows both optical excitation from the valence band into the acceptor level and from the acceptor level to the conduction band. Assuming that the upper curve corresponds to $e_p^0 = 0$ or the curve (1) in Fig. 15(d), then from this figure, we have

$$(e_n^0 + e_p^0)/e_p^0 = [6.0^2 - 5.2^2]/[6.0^2 - 5.63^2] = 2.1$$

so that $e_n^0/e_p^0 = 1.1$ at $\hbar\omega = 0.67$ eV. The values of these optical emission rates can be obtained from the time constant of the capacitance transients. At 0.59 eV, $e_n^0 = 1/\tau = 1/44\text{s} = 0.0228$/sec and at 0.67 eV, $e_n^0 + e_p^0 = 1/14.7$ sec $= 0.068$/sec. Using the ratio at 0.67 eV just obtained, then $e_p^0 = 0.032$/sec and $e_n^0 = 0.036$/sec.

Another powerful application is to demonstrate unequivocally the multiplicity of charge states of a deep level impurity. For example, it has been applied by ROSIER[6,19] to demonstrate the double donor property of sulfur impurity in silicon with energy levels of $E_C - E_{T1} = 0.30$ eV and $E_C - E_{T2} = 0.58$ eV. The $C(t)$ curve has two plateaus of equal increment when $\hbar\omega$ is increased from $0.3 < \hbar\omega < 0.58$ to $\hbar\omega > 0.58$ eV.

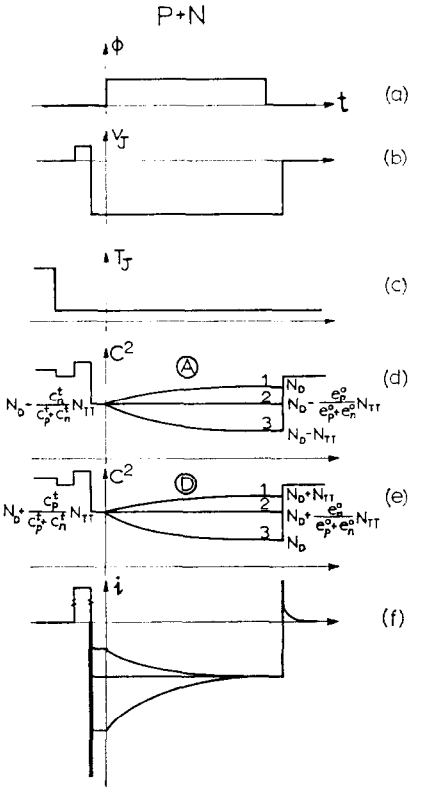

FIG. 17. Low temperature photoexperiments with carrier injection by forward junction bias, in P^+N diode.

5.2 *Experiments* 8, *carrier injection by forward bias*

The initial charge state of the impurity centers in the transition region under reverse bias can also be set by forward injection in a similar way as that in experiment 5 described in Section 4.2 and illustrated in Fig. 13. The initial condition prior to switching on the light is then determined by the ratio of the capture rates, c_n^t/c_p^t, and allows the determination of this ratio from either the capacitance or the current transient as indicated in Fig. 13, if the injection level is very high so that $N = P \gg N_D$ or N_A. The predicted transients of Fig. 13 can be applied to the present case with the thermal emission rates replaced by the optical emission rates, but retaining the thermal capture rates. A forward voltage pulse is applied to the sample in the dark at a low temperature and the illumination is turned on after the forward voltage is switched to a reverse bias, V_R and the electrical transient has died down. The sequence is illustrated in Fig. 17 and the responses for the P^+N diode structures are also indicated.

5.3 *Experiments* 9, *carrier generation by interband light*

Uniform generation of carriers can be more readily achieved by interband optical excitation with photon energy slightly above the threshold, E_G, as indicated in Section 4.3. The series resistance in the circuit reduces the junction voltage to essentially zero during the interband optical generation as indicated in Fig. 18(b) so that the carriers are not swept out due to the absence of a high field in the transition region. Other than the temporal sequence of illumination as indicated in

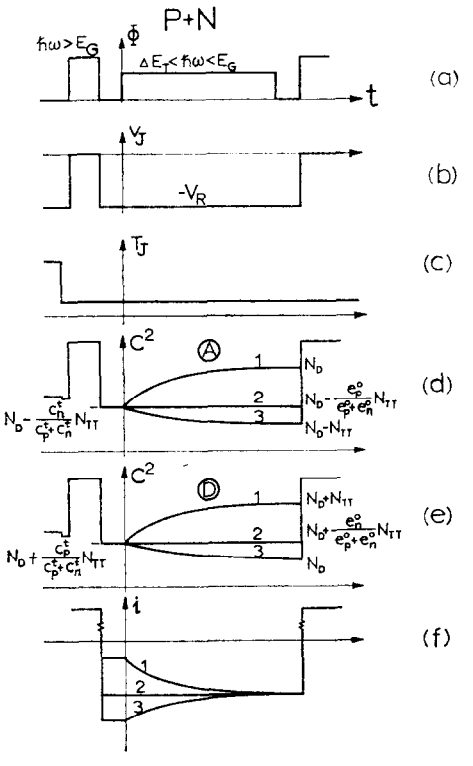

FIG. 18. Low temperature photoexperiments with carrier generation by interband light in P^+N diode.

Fig. 18(a), the transients are identical to those in Fig. 17 using forward bias injection.

The use of light with $\hbar\omega \gg E_G$ as discussed in Fig. 8 will set the initial condition of the impurity center identical to that obtained from zero bias as illustrated in Fig. 15, if light is completely absorbed in the P^+ or the N^+ layer. Thus, the results of Fig. 15 are expected. However, if the carriers are generated in a thin layer on the lightly doped side of the transition region, then a completely new set of initial conditions is obtained which cannot be achieved otherwise. Considering the P^+N case or the P^+NN^+ case, hole injection from the N^+ side would give the initial condition of $n_T(0) = 0$ and $p_T(0) = N_{TT}$ so that the initial $C^2(0)$ will have the values shown in Table 6 instead of those shown in Fig. 18. The difference between this case and the zero bias case is evident by comparing Table 6 with Table 2. The interesting results of this case is that the photocapacitance is negative for all the four combinations while the photocapacitance for the zero bias case of Fig. 15 is positive. This type of initial condition is especially useful for an acceptor impurity center in a P^+N structure whose energy level is below the midgap position since it would then allow the determination of e_p^0 and N_{TT} or N_{TT}/N_D in the range of photon energy of $E_T - E_V < \hbar\omega < E_C - E_T$ where e_n^0 is zero. This would not be possible if zero bias initial condition is used as indicated by curve (3) of Fig. 15(d), and the N^+P diode must be used as indicated by curve (3) of Fig. 15(g). Thus, the interband optical injection from one surface layer of the diode offers the versatility of setting the initial charge state to either the most negative or the most positive condition.

6. HIGH TEMPERATURE PHOTOCAPACITANCE AND PHOTOCURRENT EXPERIMENTS

The photocurrent experiment was proposed and demonstrated by SAH *et al.*[4] (previously called the impurity photovoltaic effect) as an accurate method for the determination of the thermal and optical emission rates and cross sections of electrons and holes at impurity centers in semiconductors. The details of the previously proposed method and their extensions using various means of setting the initial conditions of $n_T(0)$ are discussed in the following subsections.

6.1 *Experiments* 10, *no carrier injection*

Three types of initial conditions can be employed in these experiments with no carrier injections: (1) the dark steady state, (2) the equilibrium, and (3) band-impurity photoexcitation at a different intensity. (1) was previously proposed, (2) provides simplification and unique interpretation of results and (3) extends the light chopping rate to nanosecond speed using electro-optics.

The dark steady state initial condition. The initial condition of $n_T(0)$ is that of the dark steady state under large reverse bias. The temporal sequences of the optical and electrical switching are illustrated in Fig. 19(a–c) and the expected capacitance and current transient waveforms are shown in Fig. 10(d–f).

The initial and final conditions (assuming that $t_{ON} \gg \tau_{ON}$) of the trapped charge concentration under illumination or during turn-on transient are

$$n_T(0) = N_{TT} e_p^t / (e_n^t + e_p^t) \qquad (6.1)$$

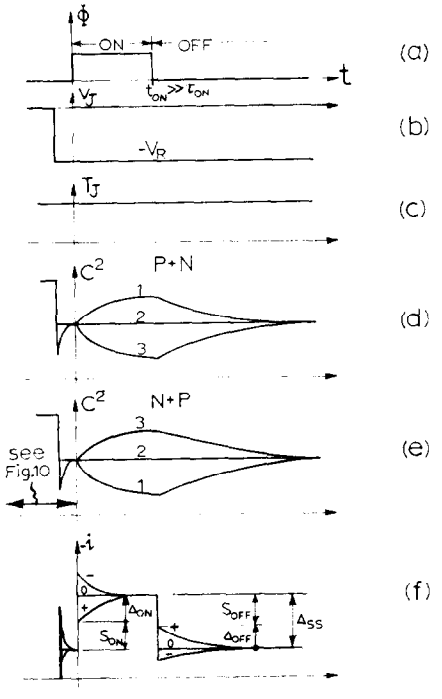

FIG. 19. High temperature photoexperiments with the dark steady state initial condition.

and

$$n_T(\infty) = N_{TT}[(e_p^0+e_p^t)/(e_n^0+e_n^t+e_p^0+e_p^t)] \qquad t_{ON} \gg \tau_{ON}. \qquad (6.2)$$

The temporal variation of the trapped electron concentration is then

$$n_T(t) = n_T(\infty)+[n_T(0)-n_T(\infty)]\exp(-t/\tau_{ON}) \qquad (6.3)$$

where

$$\tau_{ON} = 1/(e_n^0+e_n^t+e_p^0+e_p^t). \qquad (6.4)$$

The capacitance transients are very similar to those in Fig. 17. The square capacitance is proportional to $N_I(t)$ which was tabulated in Table 4. It can readily be shown using (6.1) and (6.2) that three types of capacitance transients can be observed during the turn-on transient for either a donor or acceptor like impurity center as indicated in Fig. 19(d), (e) and Fig. 20. These cases correspond to (1) $(e_n^t/e_p^t) < (e_n^0/e_p^0)$, (2) $(e_n^t/e_p^t) = (e_n^0/e_p^0)$ and (3) $(e_n^t/e_p^t) > (e_n^0/e_p^0)$.

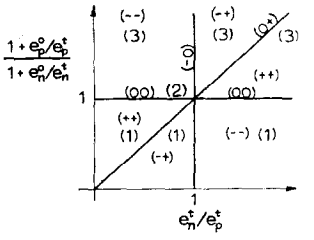

FIG. 20. The photocapacitance and photocurrent waveform map of the high temperature photoexperiments of Fig. 19. The map illustrates the effect of e_n^t/e_p^t, e_p^0/e_p^t and e_n^0/e_n^t on the waveforms shown in FIG. 19(d) to (e). (++), (+−), etc. show the (ON, OFF) portions of the current waveform. (1), (2) and show the photocapacitance wave forms.

During the turn-off transient, beginning at $t = t_{ON}$ in Fig. 19(a), the initial and final trapped electron concentrations are just those given by (6.1) and (6.2), interchanged. However, the turn-off time constant is

$$\tau_{OFF} = 1/(e_n^t+e_p^t) \qquad (6.5)$$

since this is in the dark and there is only thermal emission of electrons and holes which drives the system towards the dark steady state condition. Thus, the capacitance transient can be used to determine the sum of $e_n^t+e_p^t$ and $e_n^t+e_p^t+e_n^0+e_p^0$ and in addition a ratio e_p^t/e_p^0 or e_n^t/e_n^0 if N_D (or N_A) and N_{TT} are determined by other measurements.

The length of the dark capacitance transient due to voltage switching from $V = 0$ to $V = -V_R$, indicated in Fig. 19 for $t < 0$ and corresponding to Fig. 10, can be reduced to zero. Thus, the voltage switching to $-V_R$ and the optical excitation of impurity occur at the same time. This would set the initial condition of the charge states to the equilibrium value, $n_T(0) = N_{TT}$ for P^+N diodes and $n_T(0) = 0$ for N^+P diodes. This would not provide additional results which were not already obtained in dark capacitance transient experiments in Section 4.1 and Fig. 10, but it simplifies results and hence will be discussed in next subsection.

The photocurrent transient or the impurity photovoltaic current illustrated in Fig. 19(f) can be obtained readily from the general result given by (4.8) and (4.8A) with thermal emission rates in those expressions replaced by the total emission rates, $e_n^t+e_n^0$ and $e_p^t+e_p^0$. The photocurrent

contains two components: the conduction and the displacement currents. The latter was neglected previously.[4] Thus, the total current during the turn-on transient is given by

$$i_{ON}(t) = (qWA/2)[(e_p{}^t + e_p{}^0)p_T + (e_n{}^t + e_n{}^0)n_T] \tag{6.6}$$

$$= qWAN_{TT}[[(e_n{}^t + e_n{}^0)(e_p{}^t + e_p{}^0)/(e_n{}^t + e_n{}^0 + e_p{}^t + e_p{}^0)] + \tfrac{1}{2}[(e_n{}^0 e_p{}^t - e_n{}^t e_p{}^0)(e_n{}^t + e_n{}^0 - e_p{}^t - e_p{}^0)/(e_n{}^t + e_p{}^t)(e_n{}^t + e_n{}^0 + e_p{}^t + e_p{}^0)] \exp(-t/\tau_{ON})] \tag{6.6A}$$

for the case of constant W or low N_{TT} compared with N_D or N_A. This is also valid for arbitrary N_{TT} in a P^+IN^+ diode operated in the punch-through mode so that W is the constant I-layer width.

The turn-off transient can be readily obtained in the same way. It may be directly obtained from (6.6A) by interchanging $e_n{}^t + e_n{}^0$ with $e_n{}^t$ and $e_p{}^t + e_p{}^0$ with $e_p{}^t$.

Due to the abrupt change of the electron and hole emission rates at $t = 0$ and $t = t_{ON}$ when the light is turned on and off, corresponding current steps occur and are illustrated in Fig. 19(f). These are denoted by S_{ON} and S_{OFF} and they may be readily obtained from (6.6A) and the corresponding expression for the turn-off current and the dark steady state current given by $qN_{TT}We_n{}^t e_p{}^t/(e_n{}^t + e_p{}^t)$. These are

$$S_{ON} = qN_{TT}W(e_n{}^t e_p{}^0 + e_n{}^0 e_p{}^t)/2(e_n{}^t + e_p{}^t) \tag{6.7}$$

and

$$S_{OFF} = qN_{TT}W(e_n{}^t e_p{}^0 + e_n{}^0 e_p{}^t + 2e_n{}^0 e_p{}^0)/2(e_n{}^t + e_n{}^0 + e_p{}^t + e_p{}^0) \tag{6.8}$$

The total photocurrent transient, excluding the initial step during the turn-on and turn-off phases are denoted by Δ_{ON} and Δ_{OFF} as illustrated in Fig. 19(f). These are given by

$$\Delta_{ON} = -(qN_{TT}W/2)(e_n{}^0 e_p{}^t - e_n{}^t e_p{}^0)(e_n{}^t + e_n{}^0 - e_p{}^t - e_p{}^0)/(e_n{}^t + e_p{}^t)(e_n{}^t + e_n{}^0 + e_p{}^t + e_p{}^0) \tag{6.9}$$

and

$$\Delta_{OFF} = -(qN_{TT}W/2)(e_n{}^0 e_p{}^t - e_n{}^t e_p{}^0)(e_n{}^t - e_p{}^t)/(e_n{}^t + e_p{}^t)(e_n{}^t + e_n{}^0 + e_p{}^t + e_p{}^0). \tag{6.10}$$

Three shapes of the turn-on and turn-off current transients are possible and illustrated in Fig. 19(f). They correspond to positive (+), zero (0), and negative (−) values of Δ_{ON} and Δ_{OFF}. Only six combinations of the turn-on and turn-off transients exist which are (ON, OFF) = (00), (0+), (−0), (++), (−−) and (−+). A graph, mapping the regions of the various behaviors of both $i(t)$ and $C^2(t)$ as a function of the ratio $e_n{}^t/e_p{}^t$ and $[1+(e_p{}^0/e_p{}^t)]/[1+(e_n{}^0/e_n{}^t)]$ is given in Fig. 20.

It can readily be shown using (6.7) to (6.10) that $|\Delta_{ON}/S_{ON}| < 1$ and $|\Delta_{OFF}/S_{OFF}| < 1$. This means that the initial steps of the turn-on and turn-off transients must be greater than one half of the total steady state photocurrent: $S_{ON} \geq \Delta_{SS}/2$ and $S_{OFF} \geq \Delta_{SS}/2$.

The measurements of τ_{ON}, τ_{OFF}, S and Δ where the latter are the ratios defined by

$$S = S_{ON}/S_{OFF} = (1+E)/[1+2(e_n{}^t/e_n{}^0 + e_p{}^t/e_p{}^0)^{-1}] \tag{6.11}$$

and

$$\Delta = \Delta_{ON}/\Delta_{OFF} = 1 + (e_n{}^0 - e_p{}^0)/(e_n{}^t - e_p{}^t) \tag{6.12}$$

with $E = (e_n{}^0 + e_p{}^0)/(e_n{}^t + e_p{}^t) = (\tau_{OFF} - \tau_{ON})/\tau_{ON}$, can in principle provide enough information to determine all the four emission rates, $e_n{}^t$, $e_n{}^0$, $e_p{}^t$ and $e_p{}^0$. However, there is an ambiguity due to the symmetry of the results with respect to electrons and holes so that it is not possible to distinguish $e_n{}^0$ from $e_p{}^0$ nor $e_n{}^t$ from $e_p{}^t$. A determination of the size of the ratio $e_n{}^t/e_p{}^t$ to be either greater or less than 1 or that of $e_n{}^0/e_p{}^0$ must be made from other experimental information such as those of the previous experiments. However, once this is determined, it is evident that a knowledge of the impurity concentration is not needed since

only current ratios such as (6.11) and (6.12) are required.

To facilitate numerical calculation, (6.11) and (6.12) may be combined to give

$$e_n^0 - e_p^0 = \pm\sqrt{[1-(1+E-S)(1+E-\Delta)/E(1+E-S\Delta)](e_n^0 - e_p^0)} \quad (6.13)$$

and

$$e_n^t - e_p^t = \pm\sqrt{[1-(1+E-S)(1+E-\Delta)/E(1+E-S\Delta)](e_n^t + e_p^t)E/(\Delta-1)} \quad (6.14)$$

These can be combined with $(e_n^t + e_p^t) = \tau_{OFF}^{-1}$ and $(e_n^0 + e_p^0) = \tau_{ON}^{-1} - \tau_{OFF}^{-1}$ to give the four emission rates from the data of τ_{ON}, τ_{OFF}, S and Δ. The two signs of (6.13) and (6.14) again reflect the ambiguity due to electron–hole symmetry just stated.

Application of this method has been made to the gold acceptor level in Si *PIN* diode structures[5] giving both the temperature, electric field and photon energy dependences of the emission rates. A typical experimental data of the photocurrent is given in Fig. 21 showing two of the possible turn-on transients. The turn-off transient is always type (+) for the acceptor gold level.

Equilibrium initial condition. The use of the equilibrium initial condition for $n_T(0)$ by zero biasing the junction does not provide additional information over those already obtained from dark transient measurements in the capacitance transient experiments discussed in Fig. 19 and Fig. 10. However, this does provide considerable simplification in interpreting the photocurrent transient. In addition, it provides a unique solution since the symmetry between electrons and holes exhibited in the experiment described in Fig. 19 is now removed in the P^+N and N^+P diodes due to the complimentary but different initial conditions of $n_T(0)$ in the two structures.

The temporal sequence of switching events and the expected capacitance and current transients are shown in Fig. 22. The initial current spike, similar to those discussed in Fig. 10 are neglected. The initial condition of the trapped electron concentration during the turn-on transient phase is

$$n_T(0) = N_{TT}N_E/(N_E + n_1) \quad (6.15)$$

where N_E is equilibrium electron concentration and $n_1 = N_C \exp(E_T - E_C)/kT$ is the electron

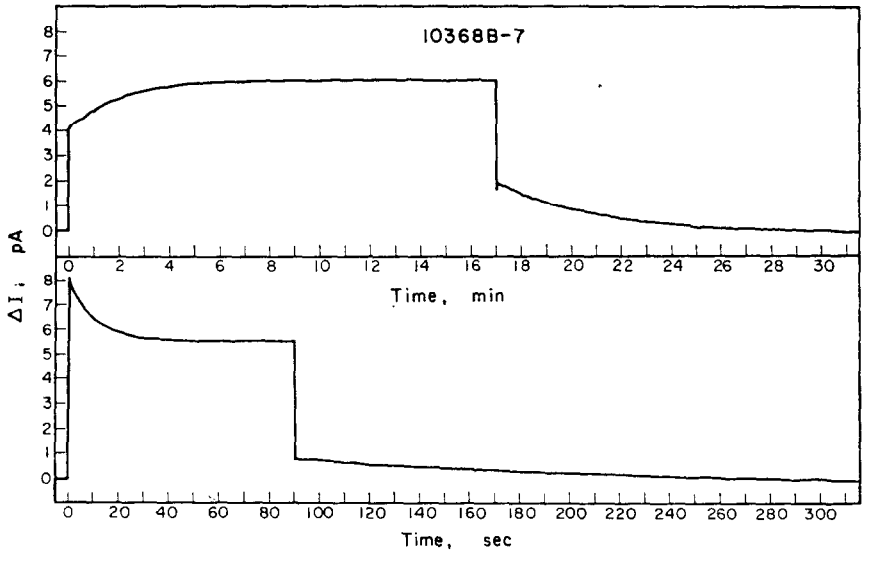

FIG. 21. Experimental recorder traces of the high temperature photocurrent waveforms illustrating two types of behaviors.

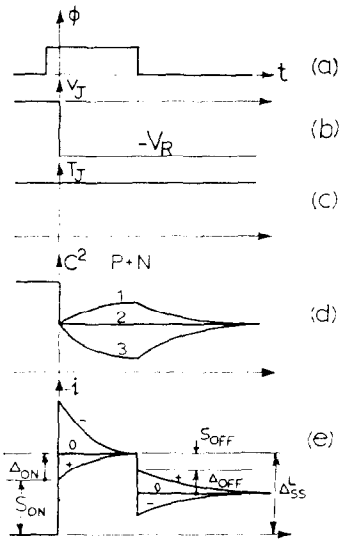

FIG. 22. High temperature photoexperiments with equilibrium initial condition.

concentration when the Fermi level coincides with the energy level of the center, E_T. This is the only difference between this case and that given in (6.1) to (6.4). The shape of the turn-on current transient has again three forms similar to those in Fig. 19(f), however, the conditions on the ratios e_n^t/e_p^t, e_n^0/e_n^t and e_p^0/e_p^t to give these three wave forms are different from those in Fig. 19(f). The current wave forms are labeled in the same way as in Fig. 19(f) and given in Fig. 21(e). Using (6.15) in (6.6), the initial current step is then

$$S_{ON} = (qWN_{TT}A/2)[(e_p^t+e_p^0)n_1/(N_E+n_1)+(e_n^t+e_n^0)N_E/(N_E+n_1)] \quad (6.16)$$

$$= (qWN_{TT}A/2)(e_n^t+e_n^0) \quad (P^+N \text{ diode}) \quad (6.16A)$$

$$= (qWN_{TT}A/2)(e_p^t+e_p^0) \quad (N^+P \text{ diode}). \quad (6.16B)$$

The total steady state photocurrent excluding the initial step is then

$$\Delta_{ON} = (qN_{TT}WA/2)[(e_n^t+e_n^0)(e_p^t+e_p^0-e_n^t-e_n^0)/(e_n^t+e_n^0+e_p^t+e_p^0)] \quad (P^+N \text{ diode}) \quad (6.17A)$$

$$= (qN_{TT}WA/2)[(e_p^t+e_p^0)(e_n^t+e_n^0-e_p^t-e_p^0)/(e_n^t+e_n^0+e_p^t+e_p^0)]. \quad (N^+P \text{ diode}). \quad (6.17B)$$

Thus, $|S_{ON}/\Delta_{ON}| = |(1+e_n/e_p)/(1-e_n/e_p)| > 1$ for P^+N diode and similarly with e_n and e_p interchanged, $|S_{ON}/\Delta_{ON}| > 1$ for N^+P diode. Here $e_n = e_n^t+e_n^0$, etc. Thus, the initial current step must be greater than 1/2 of the final steady state photocurrent, a result identical to that in Fig. 19(f).

The condition for the (−), (0) and (+) waveforms of the turn-on photocurrent transient is simply indicated in (6.17A) for the corresponding three cases of $\Delta_{ON} < 0$, $\Delta_{ON} = 0$ and $\Delta_{ON} > 0$. For the P^+N diode, these correspond to $e_p^t+e_p^0 \lesseqgtr e_n^t+e_n^0$. A similar set of conditions can be obtained for the N^+P case.

A particularly simple result is obtained for S_{ON}/Δ_{SS}^L which are

$$S_{ON}/\Delta_{SS}^L = [1+(e_n^t+e_n^0)/(e_p^t+e_p^0)]/2 \quad (P^+N \text{ diode}) \quad (6.18A)$$

$$= [1+(e_p^t+e_p^0)/(e_n^t+e_n^0)]/2 \quad (N^+P \text{ diode}). \quad (6.18B)$$

Thus, a measurement of this ratio will give the ratio $(e_n^t+e_n^0)/(e_p^t+e_p^0)$ uniquely.

The turn-off transient is identical to those discussed in Fig. 19(f) and the results given by (6.8) and (6.10) can be used here.

There are again six possible combinations of the turn-on and turn-off wave forms for either the P^+N or the N^+P diode. These are related to the ratios of the thermal and optical emission rates and are mapped in Fig. 23 using the same coordinates as those in Fig. 19(g).

To evaluate all four emission rates from the data, the technique used in Fig. 19 can be employed but with considerable simplification, Consider the alternative measurement of the ratios given by (6.18A) or (6.18B). These may be combined with the turn-on time constant

$$\tau_{ON} = 1/(e_n^t+e_n^0+e_p^t+e_p^0)$$

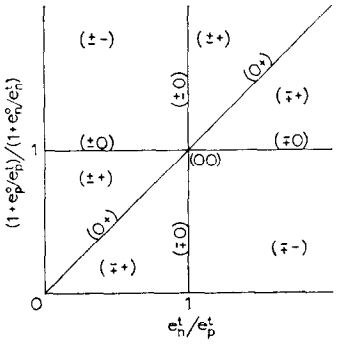

FIG. 23. The waveform map of the photocurrent transient of Fig. 22(e). The upper sign of $(\pm X)$ is for P^+N junction and the lower sign for N^+P junction.

to give

$$e_p{}^t + e_p{}^0 = \Delta_{SS}{}^L/2S_{ON}\tau_{ON} \qquad (P^+N \text{ diode}) \qquad (6.19A)$$

$$e_n{}^t + e_n{}^0 = \Delta_{SS}{}^L/2S_{ON}\tau_{ON} \qquad (N^+P \text{ diode}) \qquad (6.19B)$$

Since $e_n{}^0$ and $e_p{}^0$ are directly proportional to the photon flux, both $e_n{}^t$ and $e_n{}^0$ or $e_p{}^t$ and $e_p{}^0$ can be obtained by varying the photon flux or light intensity in the experiment.

Band-impurity photoexcitation at lower level. This is the third type of initial condition. The monochromatic light is chopped electro-optically to give two constant light intensity levels and the durations of the two light levels are sufficiently long so that all transients have passed during the two durations. We suppose that the light levels are Φ_H and Φ_L. The corresponding optical emission rates are $e_n{}^{0H}$, $e_p{}^{0H}$, $e_n{}^{0L}$ and $e_p{}^{0L}$. The solutions obtained for the case with dark steady state initial condition given in (6.7) to (6.14) can all be applied here provided that the following substitutions are made: $e_n{}^0 = e_n{}^H - e_n{}^L$, $e_p{}^0 = e_p{}^H - e_p{}^L$, $e_n{}^t = e_n{}^L$ and $e_p{}^t = e_p{}^L$. Here, $e_n{}^H = e_n{}^t + e_n{}^{0H}$, $e_n{}^L = e_n{}^t + e_n{}^{0L}$, etc. are the total electron (and hole) emission rates for the High and Low light level durations.

6.2 *Experiment* 11, *carrier injection by forward bias*

The initial charge condition of the impurity centers in $0 < x < W$ can be set by forward bias injection of minority carriers across the junction prior to the photocurrent and photocapacitance excitation. The sequence of the switching and the resultant transient wave forms are similar to those of Section 5.2 at low temperatures except that thermal emission of electrons and holes from the impurity centers must now be taken into account. Thus, the optical emission rates, $e_p{}^0$ and $e_n{}^0$, shown in Fig. 17(d) and (e) are to be replaced by $e_p{}^0 + e_p{}^t$ and $e_n{}^0 + e_n{}^t$ respectively.

6.3 *Experiment* 12, *carrier generation or injection by interband light*

The two methods of setting the initial condition by interband optical generation of carriers in $0 < x < W$ using $\hbar\omega > E_G$ and in the surface layer using $\hbar\omega \gg E_G$ can be employed here. The former case provides the initial condition of $n_T(0) = N_{TT}c_n{}^t/(c_n{}^t + c_p{}^t)$ if $N \doteq P \gg N_D$ (or N_A). The latter can provide a variety of initial conditions as indicated in Section 5.3. These methods would allow the determination of $c_n{}^t/c_p{}^t$ and their values at high temperatures although the dark high temperature experiments discussed in Section 4.3 are more direct.

7. CONCLUDING REMARKS

A detailed analysis has been given of a number of methods using the p–n junction current and high frequency capacitance for the determination of the electronic properties of impurity centers in semiconductors. It is shown that a combination of several of these experiments can provide a unique experimental determination of energy level of the impurity center, its multiplicity of charge states, the thermal capture rates, the thermal and optical emission rates and cross sections of electrons and holes at the impurity center. The temperature, electric field and photon energy dependences of these rates and cross sections can also be determined which may be used to provide information of the nature of the impurity potential in a semiconductor lattice. These methods not only can provide highly accurate data for these fundamental atomic parameters of an impurity center which have not been possible previously, they may also be used as quantitative analysis techniques for the detection of a minute amount of impurities in semiconductors. For this application using the dark or photocapacitance techniques described in Sections

3.1 and 5.1, sensitivity of 10^{11} atoms/cm^3 can be achieved. For a p–n junction with an area of 10^{-3} cm^2 a transition layer width of 10^{-4} cm, the total detectable number of impurity atom is $10^{11}\times 10^{-3}\times 10^{-4} = 10^5$ atoms.[19]

REFERENCES

1. For a review of earlier literature, see Ref. 2. More recent data and references are contained in the paper by A. ONTON, P. FISHER and A. K. RAMDAS, *Phys. Rev.* **163,** 686 (1967).
2. R. H. BUBE, *Photoconductivity of Solids.* Wiley, New York (1960).
3. M. LAX, *J. Phys. Chem. Solids* **8,** 66 (1959); *Phys. Rev.* **119,** 1502 (1960). An extensive compilation of published data was also given by E. SCHIBLI and A. G. MILNES, *Mat. Sci. Engng.* **2,** 229 (1967/68).
4. C. T. SAH, A. F. TASCH, JR. *Phys. Rev. Lett.* **19,** 69 (1967) and C. T. SAH, A. F. TASCH, JR. and D. K. SCHRODER, *ibid.* **71,** (1967).
5. A. F. TASCH, JR. and C. T. SAH, *Phys. Rev.* Jan., 15 (1970).
6. L. L. ROSIER and C. T. SAH, to be published.
7. C. T. SAH, *IEEE Trans.* **ED–13,** 839 (1966).
8. L. FORBES and C. T. SAH, *IEEE Trans. Electron Devices,* **ED–16,** 1036 (1969).
9. C. B. COLLINS, R. O. CARLSON and C. J. GALLAGHER, *Phys. Rev.* **105,** 1168 (1957).
10. R. R. SENECHAL and J. J. BASINSKI, *J. appl. Phys.* **39,** 3723 (1968).
11. F. A. TRUMBORE, *Bell Syst. tech. J.* **39,** 205 (1960).
12. R. H. KINGSTON, *Proc. Instn Radio Engrs* **42,** 829 (1954); B. LAX and S. F. NEUSTADTER, *J. appl. Phys.* **25,** 1148 (1954).
13. R. WILLIAMS, *J. appl. Phys.* **37,** 3411 (1966).
14. W. D. DAVIS, *Phys. Rev.* **114,** 1006 (1959).
15. C. T. SAH, L. FORBES, L. L. ROSIER, A. F. TASCH, JR. and A. B. TOLE, *Appl. Phys. Lett.* **15,** 145 (1969).
16. S. SATO and C. T. SAH (to be published).
17. L. D. YAU and C. T. SAH, *Solid-St. Electron.* (*in press*).
18. C. T. SAH and W. SHOCKLEY, *Phys. Rev.* **109,** 1103; C. T. SAH, *Proc. IEEE* **55,** 654 (1967).
19. C. T. SAH, L. L. ROSIER and L. FORBES, *Appl. Phys. Lett,* **15,** 161, 316 (1969).

APPENDIX A

The high frequency capacitance of a P^+N junction containing a high concentration of deep-level impurity such that $N_t = N_D - N_{TT}$ and N_{TT} cannot be neglected will be given here. Supposing that a staircase charge distribution is assumed for large reverse bias, and assuming complete depletion ($N = P = 0$) and acceptor-like deep level impurity center, then the net charge distribution is

$$\rho(x) = q[N_D - N_{TT}e_n{}^t/(e_n{}^t + e_p{}^t)] \text{ in } 0<x<x_t,$$

$$\rho(x) = qN_D \text{ in } x_t<x<W \text{ and } \rho(x) = 0 \; x>W.$$

The total depletion or transition layer width is then given by [$\alpha = e_n{}^t/(e_n{}^t+e_p{}^t)$]

$$W = \frac{N_{TT}(1-\alpha)}{N_D-\alpha N_{TT}}\sqrt{\left[\frac{2K_s\epsilon_0\phi_t}{q(N_D-N_{TT})}\right]} + \frac{\sqrt{\{2K_s\epsilon_0[(N_D-\alpha N_{TT})(V_D+V_R)-N_{TT}(1-\alpha)\phi_t]/q\}}}{(N_D-\alpha N_{TT})}$$

and the high frequency capacitance of the junction can be obtained from $C = K_s\epsilon_0 A/W$. This differs from the approximate result used in the text by a small amount due to the width $W-x_t$ whose potential drop is a constant given by $(E_T-E_i)/q$. Thus, at large applied reverse bias, this can be neglected.